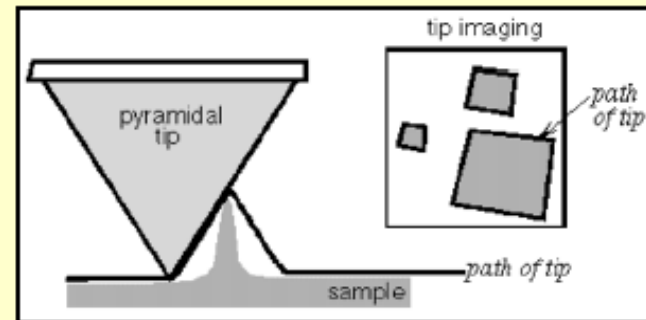
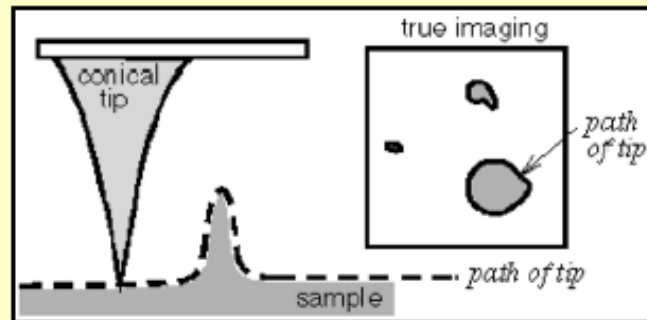


## Lecture 14: Improved lateral resolution of AFM imaging for DNA and other small bio-species

- AFM imaging resolution depends on the tip: how to make a smaller, sharper tip while still maintaining the sufficient stiffness for scanning.
- Use DNA as a good example to calibrate the lateral resolution of the AFM modified with new tips, since DNA possesses small, uniform dimensional size.
- Highly organized nanostructures self-assembled from DNA strands represent a unique approach for nanoscale patterning, especially for single-molecule control and study of bio-related processes.

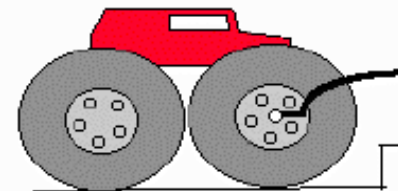
# Lateral resolution depends on tip sharpness



This profile...



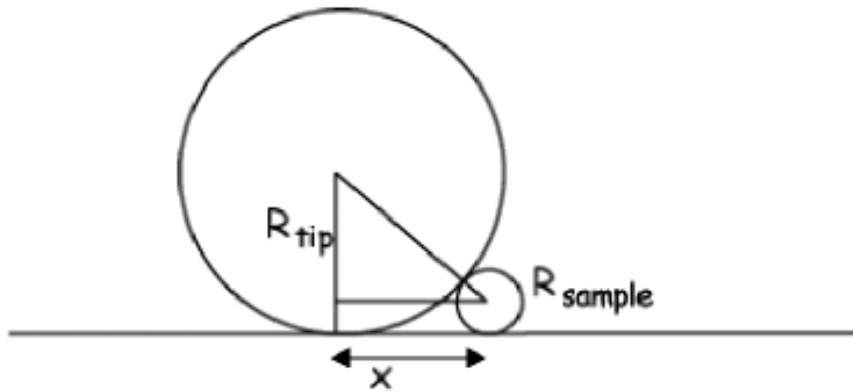
can be made with this monster...



or with this bug!



# Fat-tip Effect: *apparent width measured by large tip*



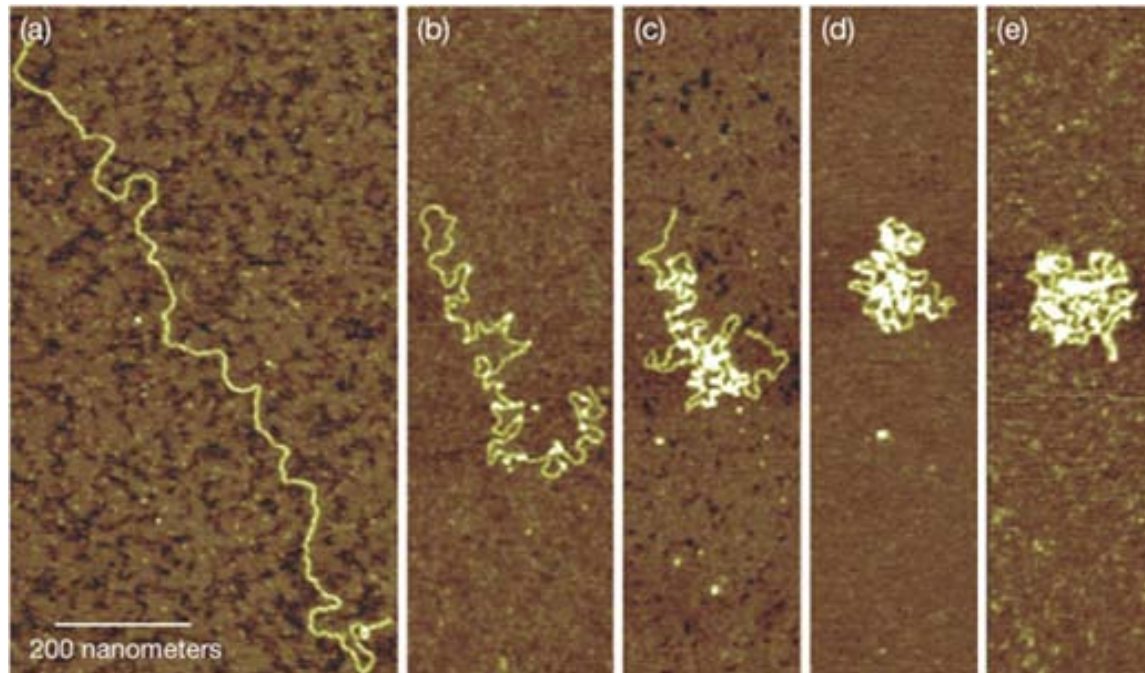
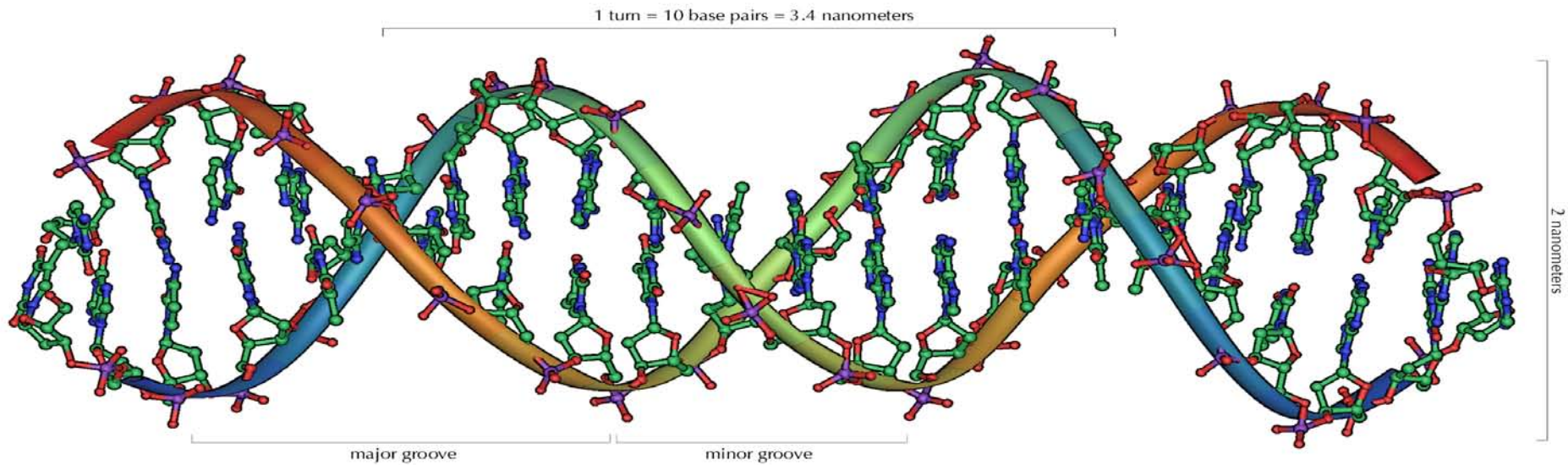
$$x^2 = (R_{tip} + R_{sample})^2 - (R_{tip} - R_{sample})^2$$

$$x^2 = \cancel{R_{tip}^2} + 2R_{tip}R_{sample} + \cancel{R_{sample}^2} - \cancel{R_{tip}^2} + 2R_{tip}R_{sample} - \cancel{R_{sample}^2}$$

$$x = 2\sqrt{R_{tip}R_{sample}}$$

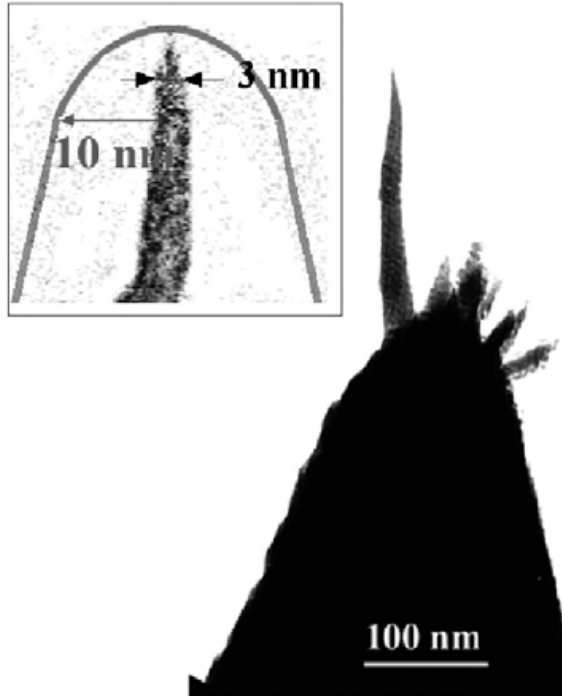
$$w = 2x = 4\sqrt{R_{tip}R_{sample}}$$

- Measured width: distance between the 1<sup>st</sup> and last tip/sample contact;
- The smaller the tip ( $R_{tip}$ ), the smaller the measured width;
- When  $R_{tip} \sim \frac{1}{4} R_{sample}$ , measured width =  $2R_{sample}$ ;
- For a 5 nm feature (say a particle), the tip apex size must be  $\sim 1$  nm to get a reliable lateral measurement --- **quite challenging!**
- Normal tip size,  $\sim 20$  nm or larger.
- Another challenge for lateral imaging: to differentiate two adjacent features.



- DNA is really small (2 nm for the double helix), soft and foldable, non-conductive, not suited E-microscopy.
- AFM imaging is good for DNA imaging, but needs significant improvement in tip-resolution.
- High resolution imaging of DNA structures is almost exclusively done by **solution AFM imaging on freshly cleaved mica**.

# Approach 1: coating with carbon spikes



High-resolution AFM tips were prepared by plasma-assisted growth of carbon spikes at the apex of Olympus AC160TS Si probes with force constant 42 N/m and resonant frequency 300 kHz. This growth did not change the force/frequency parameters of the cantilevers.

**Figure 1.** Transmission electron microscope image of the high-resolution AFM tip (length  $\sim 200$  nm, apex radius  $\sim 1$  nm). The inset is a magnified image of the end of the most protruding tip, demonstrating its small effective diameter as compared to the diameter of a typical Si commercial tip (radius = 10 nm, continuous line).

# Approach 1: coating with carbon spikes

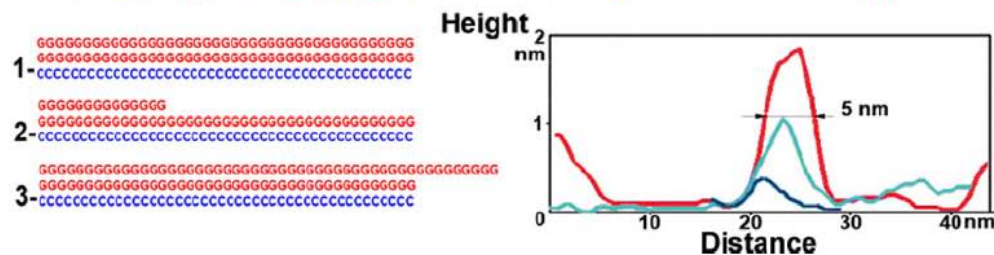
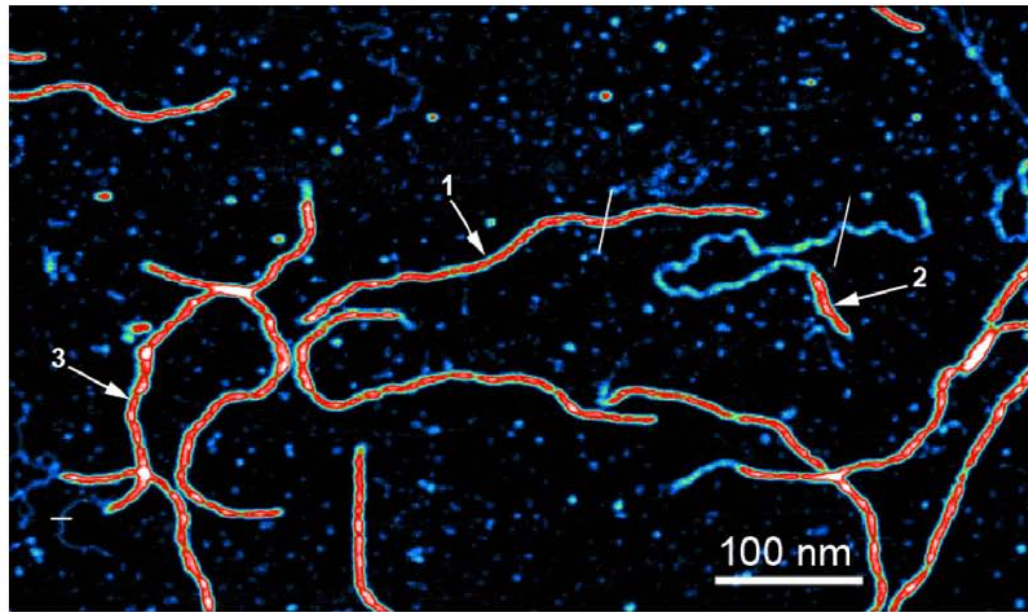


**Figure 2.** High-resolution AFM image of poly(dG)–poly(dG)–poly(dC) triplex DNA. Notice the single-strand (dark blue), double-strand (light blue) and triple-strand (red) regions in the molecules. The bottom-right inset is a cross-section of triplex, dsDNA and ssDNA regions in the molecule, taken at the short unmarked lines in the image. Bottom-left diagrams present schematic views of three types of molecules, as indicated by the arrows: 1, full-length or ‘completed’ triplex molecule; 2, ‘partially-synthesized’ triplex, containing both triplex and dsDNA fragments; 3, ‘over-synthesized’ triplex, containing a single-stranded fragment at the end of the molecule.

# Approach 1: coating with carbon spikes

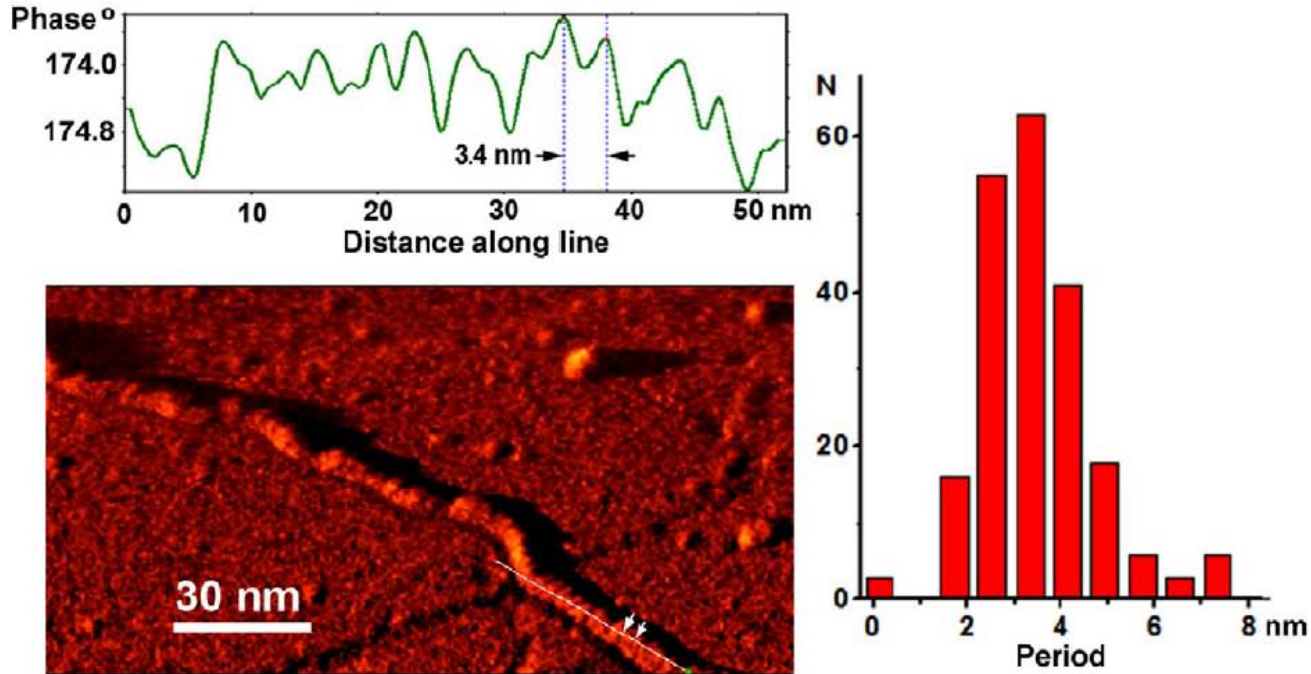
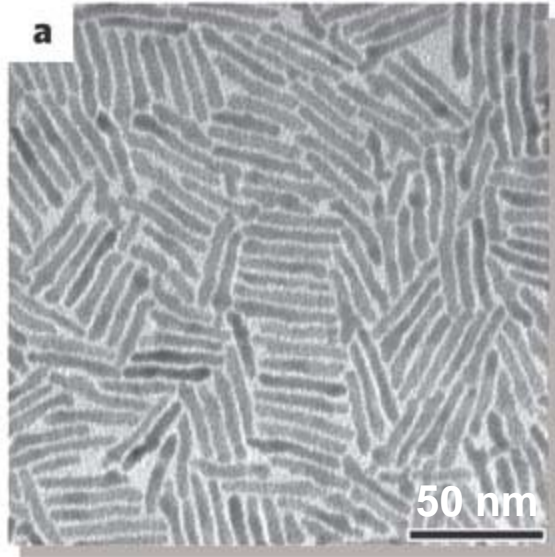


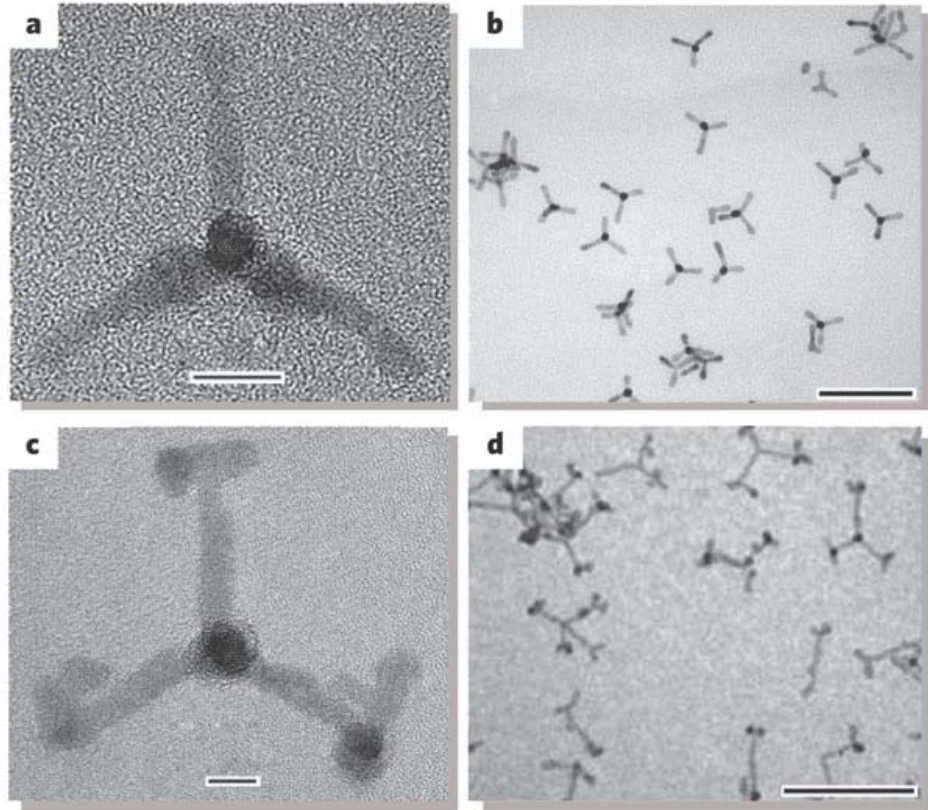
**Figure 7.** Left: high-resolution AFM *phase* image of poly(dG)–poly(dG)–poly(dC) triplex DNA. The top graph shows a cross-section of the image along the white line (at the bottom part of the image). Right: histogram of distances between adjacent peaks on cross-sections taken on many molecules (overall >200 values); the average distance is 3.4 nm (SD = 0.9 nm).

The average distance measured (3.4 nm) is consistent with the length of periodic motif of the triplex DNA ( $3.9 \pm 0.1$  nm) determined using NMR and x-ray diffraction studies.

## Approach 2: attached with nanorods



*Nano Lett.* **2**, 558–560 ( 2002)

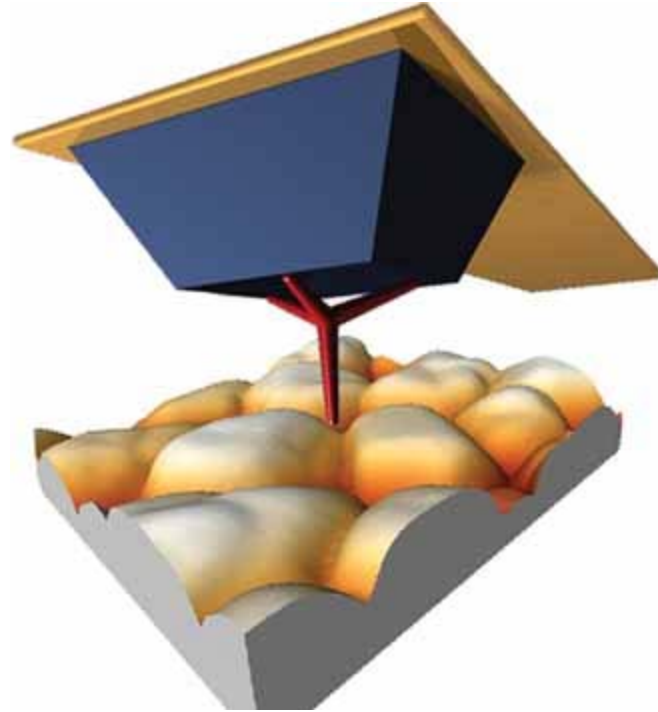


*Nature* **430**, 190–195 ( 2004)

- Inorganic semiconductor (e.g., CdSe) nanorods provide hardness and small size, but difficult to be attached to the tip;
- Tetrapods in the shape as shown above are suited for anchoring onto the tip.

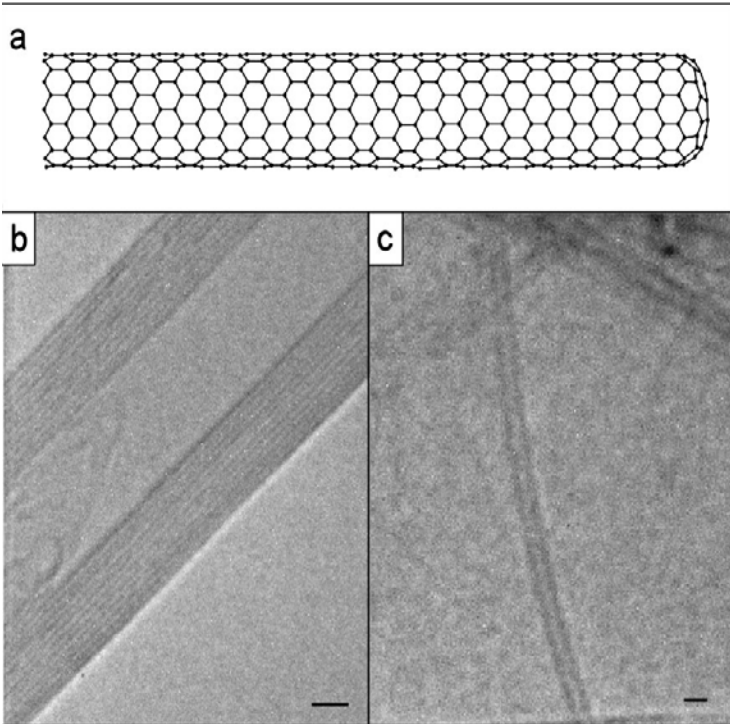


## Approach 2: attached with tetrapods



Probe Tips Functionalized with Colloidal Nanocrystal Tetrapods for High-Resolution Atomic Force Microscopy Imaging

## Approach 3: attached with carbon nanotube



(a) Truncated stick model of a single-wall nanotube (SWNT). Each hexagonal vertex corresponds to a  $sp^2$ -hybridized carbon atom.

TEM images showing the cross sectional structures of (b) a multi-wall nanotube (MWNT) and (c) a SWNT (scale bar, 2 nm).

nature  
nanotechnology

4, 483 - 491 (2009).

REVIEW ARTICLE

PUBLISHED ONLINE: 13 JULY 2009 | DOI: 10.1038/NNANO.2009.154

# Carbon nanotube tips for atomic force microscopy

Neil R. Wilson<sup>1</sup> and Julie V. Macpherson<sup>2\*</sup>

---

# *Advantages of SWNT*

- The diameter of SWNTs can be as small as 0.4 nm, typically 1-2 nm.
  - The cylindrical structure of carbon nanotubes makes it possible to image high aspect ratio samples.
  - The extremely high Young's modulus of carbon nanotubes, enables very small diameter and high aspect ratio tubes to be sufficiently stable for imaging at room temperature.
  - Carbon nanotubes can reversibly buckle under high load without wear, reducing damage to both the tip and the sample.
  - The ends of carbon nanotube tips can be chemically modified for *high-resolution functional imaging*.
-

# Preparation of nanotube tips

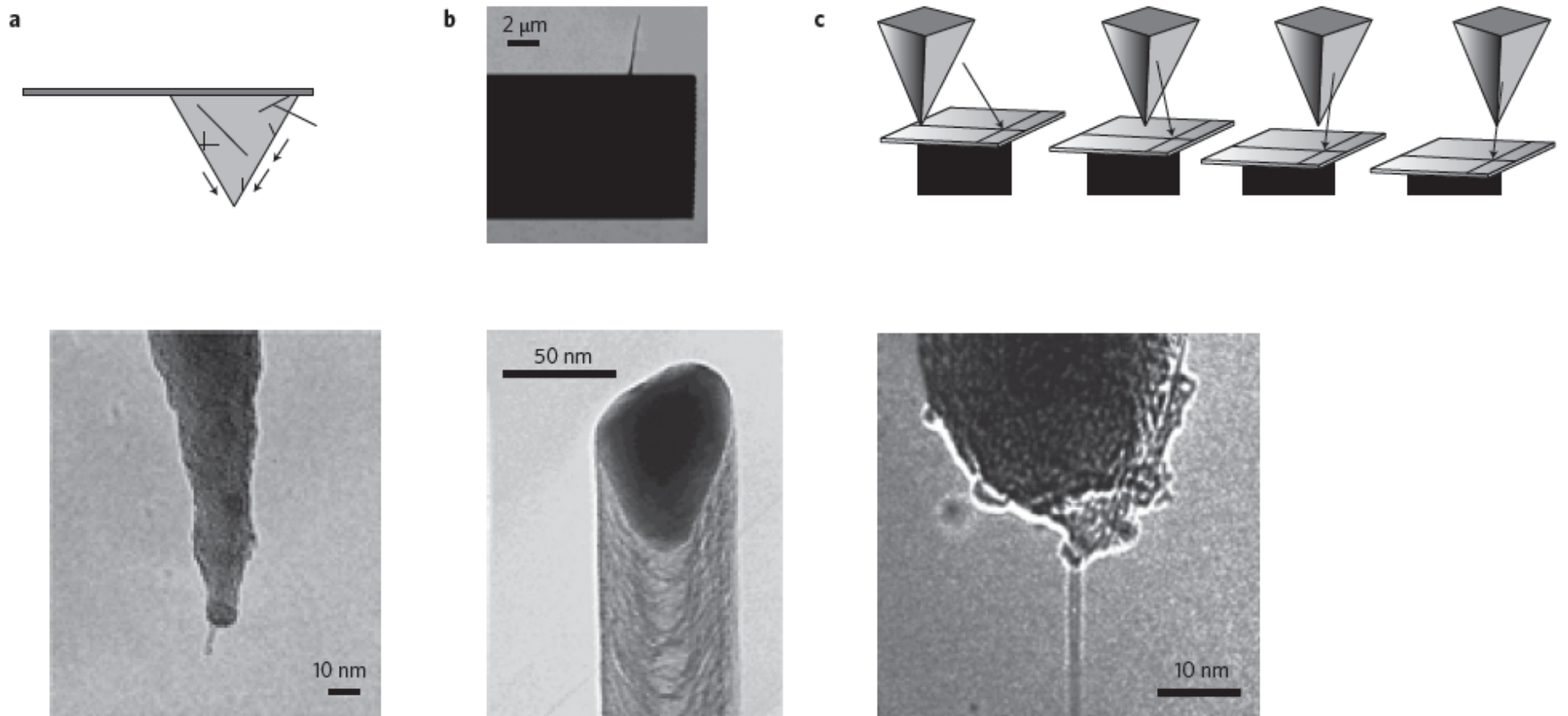


**Figure 1 | Preparation of nanotube tips.** **a**, Surface growth cCVD nanotube tip preparation. Top: Schematic of the growth process. Bottom: TEM image of an individual SWNT tip produced using this technique. Reproduced with permission from ref. 49 (© 2000 Elsevier). **b**, Cross-sectional TEM images of an individual bamboo morphology nanotube on a cantilever produced by directional-growth plasma-enhanced CVD. Top: 90° side view with  $\times 1,500$  magnification. The nanotube has a 60-nm tip diameter, is 5  $\mu\text{m}$  long, and has a tilt angle of  $13^\circ$  with respect to the cantilever. Bottom: Nanotube tip end. The nickel catalyst wrapped within thin graphite layers is clearly visible. Reproduced with permission from ref. 24 (© 2004 ACS). **c**, Nanotube attachment through 'pick-up'. Top: Schematic depicting the process by which a microfabricated pyramidal tip picks up a vertically aligned carbon nanotube. Bottom: TEM image of a 0.9-nm-diameter SWNT tip produced by 'pick-up'. Reproduced with permission from ref. 21 (© 2001 Elsevier).

# Coated nanotube tips

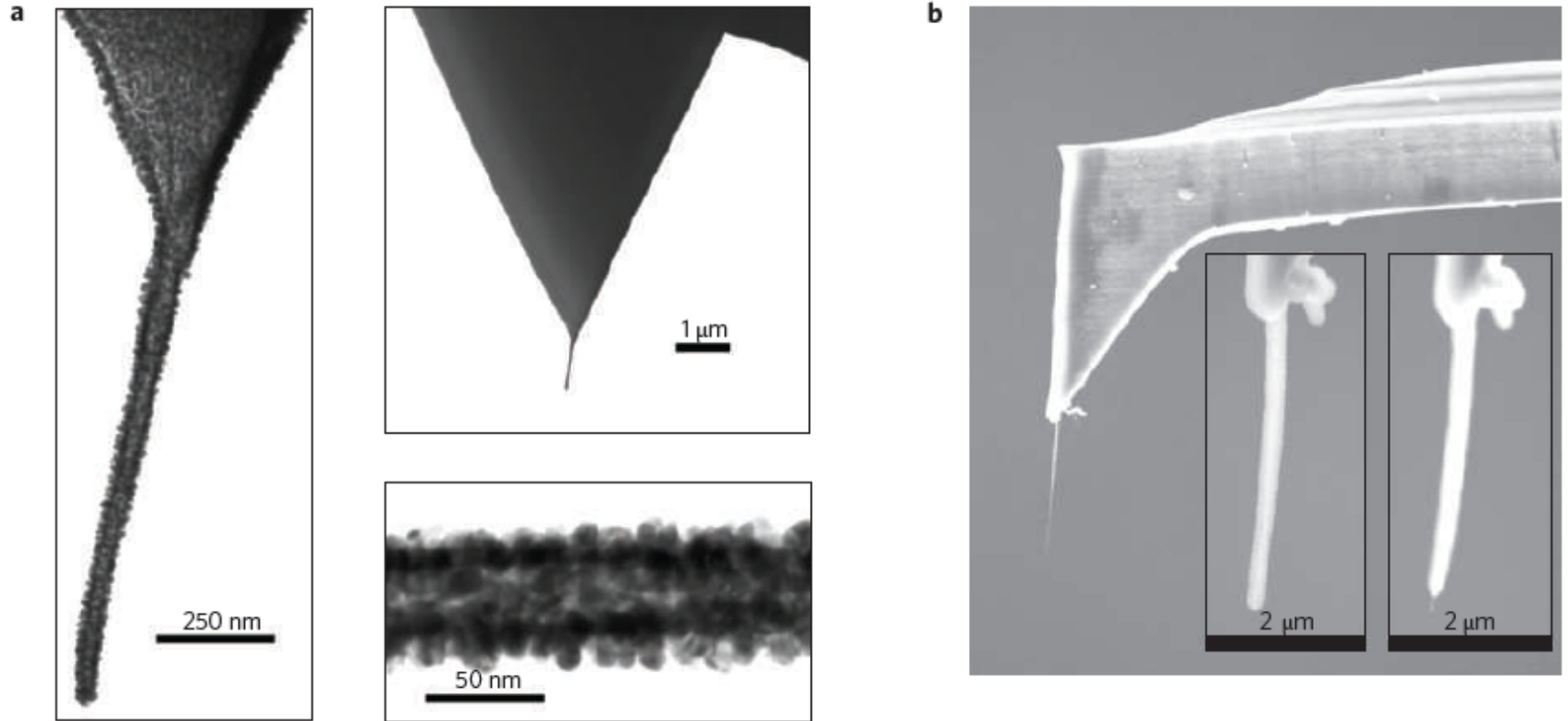
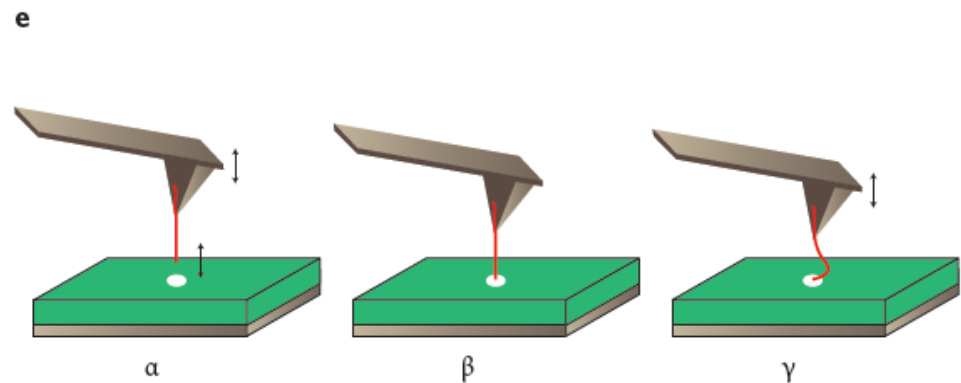
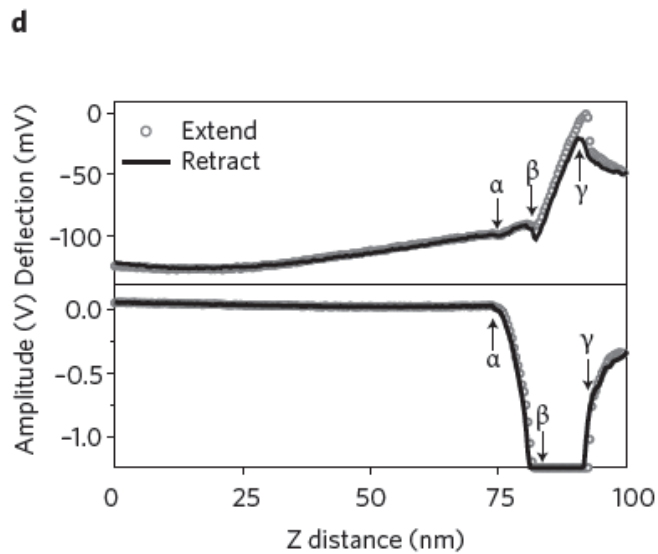
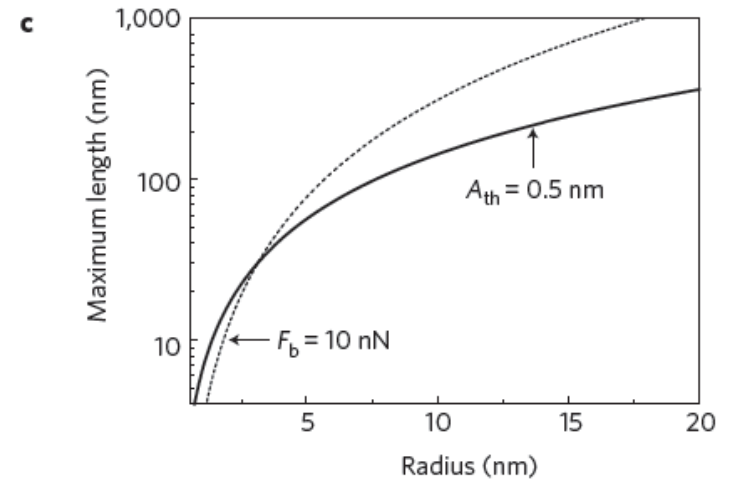
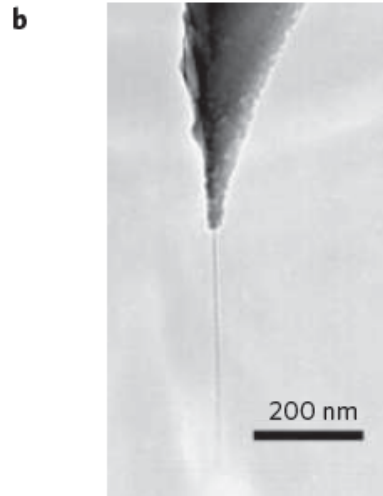
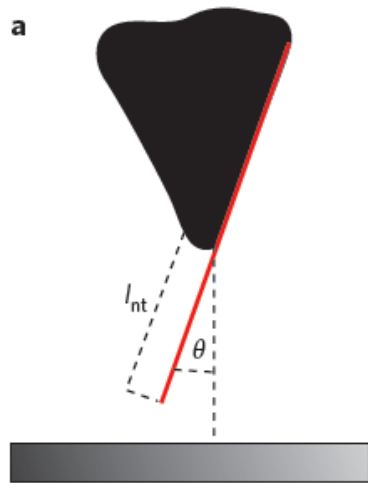


**Figure 2 | Coated nanotube AFM probes.** **a**, TEM images of a gold nanowire probe formed by sputtering onto a nanotube tip (left) and an enlarged view of the nanowire (top and bottom right). Reproduced with permission from ref. 38 (© 2003 ACS). **b**, Polymer (Parylene C)-coated nanotube tip, with the apex exposed using a laser (right inset). Reproduced with permission from ref. 85 (© 2004 ACS).

# Characterizing a nanotube tip



# Characterizing a nanotube tip: interpretation

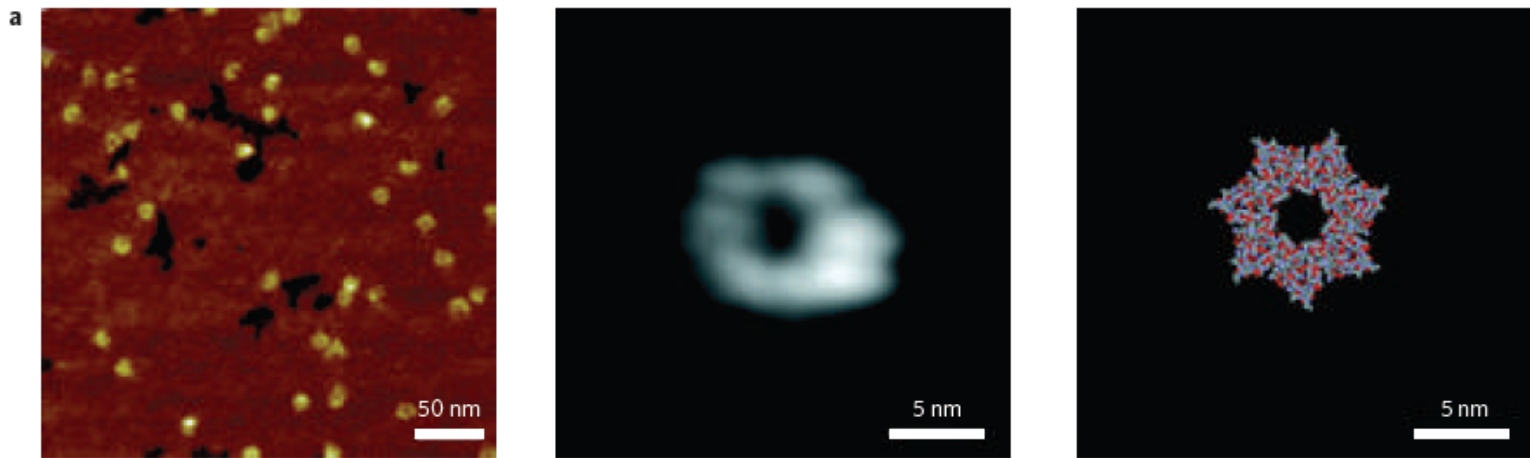
Nanotube tips are characterized by their length,  $l_{nt}$ , and angle relative to the surface,  $\theta$  (panel **a**). The nanotube radius,  $r_{nt}$ , limits the spatial resolution and has an impact on the usable length of the nanotube tip. The nanotube acts as a beam clamped at one end, and as such it will buckle when the axial load exceeds the buckling force,  $F_b$ . Panel **b** shows a transmission electron microscope (TEM) image of a nanotube tip<sup>89</sup>; the blurring of the lower portion of the nanotube is due to thermally induced oscillations (with amplitude  $A_{th}$ ). Combining continuum mechanics and the equipartition theory, it is trivial to find the following parameters:

$$F_b = \frac{\pi^2 \alpha_{nt}}{l_{nt}^2}, \quad k_l = \frac{3\alpha_{nt}}{l_{nt}^3}, \quad \alpha_{nt} = \frac{Y_{nt}\pi r_{nt}^4}{4}, \quad A_{th} = \sqrt{\frac{k_B T}{k_l}},$$

where  $k_l$  is the nanotube's lateral spring constant,  $\alpha_{nt}$  the flexural rigidity,  $Y_{nt}$  Young's modulus,  $k_B$  Boltzmann constant and  $T$  the temperature. For robust imaging,  $A_{th} < 0.5$  nm and  $F_b > 10$  nN; these constraints are plotted in **c** using  $Y_{nt} = 1$  TPa and  $T = 300$  K.

This simple model is only a guide. However the constraints on the usable length are clear: a nanotube with  $r_{nt} = 0.5$  nm should be shortened to  $l_{nt} \leq 10$  nm, whereas at  $r_{nt} = 10$  nm,  $l_{nt} \leq 1$   $\mu$ m. For a nanotube tip composed of a bundle of nanotubes, the effective Young's modulus is much lower than 1 TPa (ref. 90), however the trend of a thicker bundle allowing greater  $l_{nt}$  holds true. Coating the nanotube tip increases the flexural rigidity and so also allows greater  $l_{nt}$  (refs 38, 85).

The tapping mode force–distance curve characteristic of a nanotube tip<sup>89</sup> (**d**) and a corresponding schematic (**e**) are shown. 'Extend' and 'retract' refer to the tip being moved towards and away from the surface, respectively. At point  $\alpha$  the nanotube tip contacts the surface at the bottom of the tip oscillation. As it is lowered further the amplitude decreases until at  $\beta$  the oscillation is damped completely and the cantilever deflects. The axial force on the nanotube increases until at point  $\gamma$  the force exceeds  $F_b$ , the nanotube buckles and the tip oscillates again. The reversibility of the buckling, evident from the observation that 'retract' matches 'extend', is a distinctive signature of a nanotube tip<sup>5</sup>.



### Chaperonin protein GroES

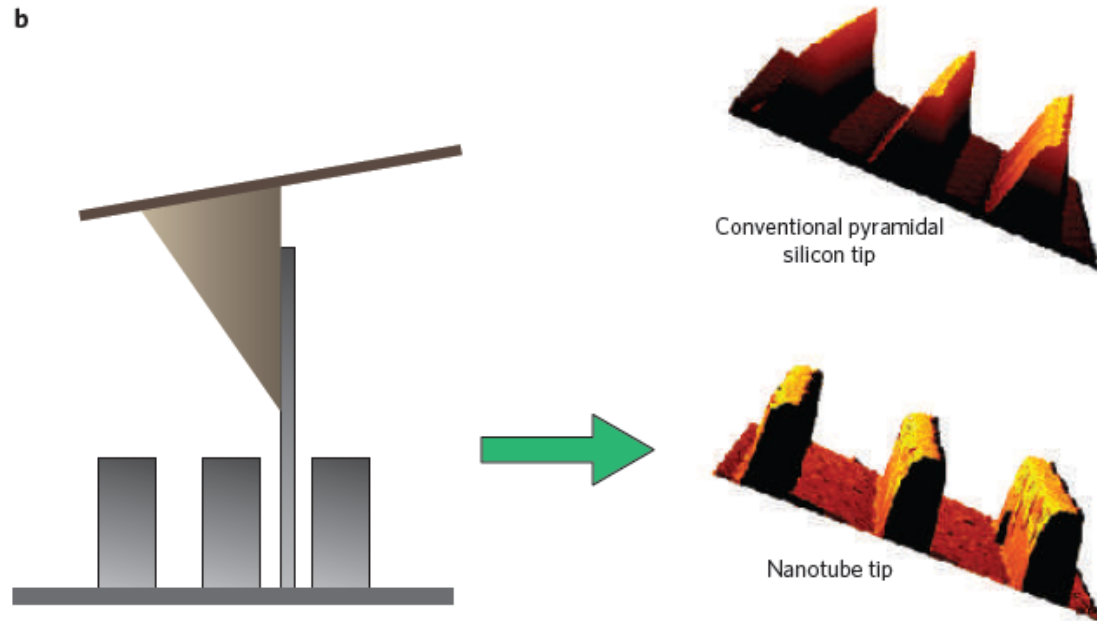


**Figure 3 | Topographical demonstrations with nanotube tips.** **a**, High-resolution imaging. The chaperonin protein GroES, imaged with a cCVD surface-grown SWNT tip. The large scan area in the left image shows both 'dome' and 'pore' conformations, representing the two sides of GroES facing up. A higher resolution image of the pore side (middle) shows the heptameric symmetry, which matches well with the crystal structure shown on the right. Reproduced with permission from ref. 52 (© 2000 PNAS). **b**, A comparison of AFM images of 280-nm-spaced, 300-nm-deep trenches in photoresist obtained with a conventional silicon probe and a nanotube probe. The improvement in the ability of the nanotube tip to map surface topography is clearly evident. Adapted with permission from refs 58 and 91.



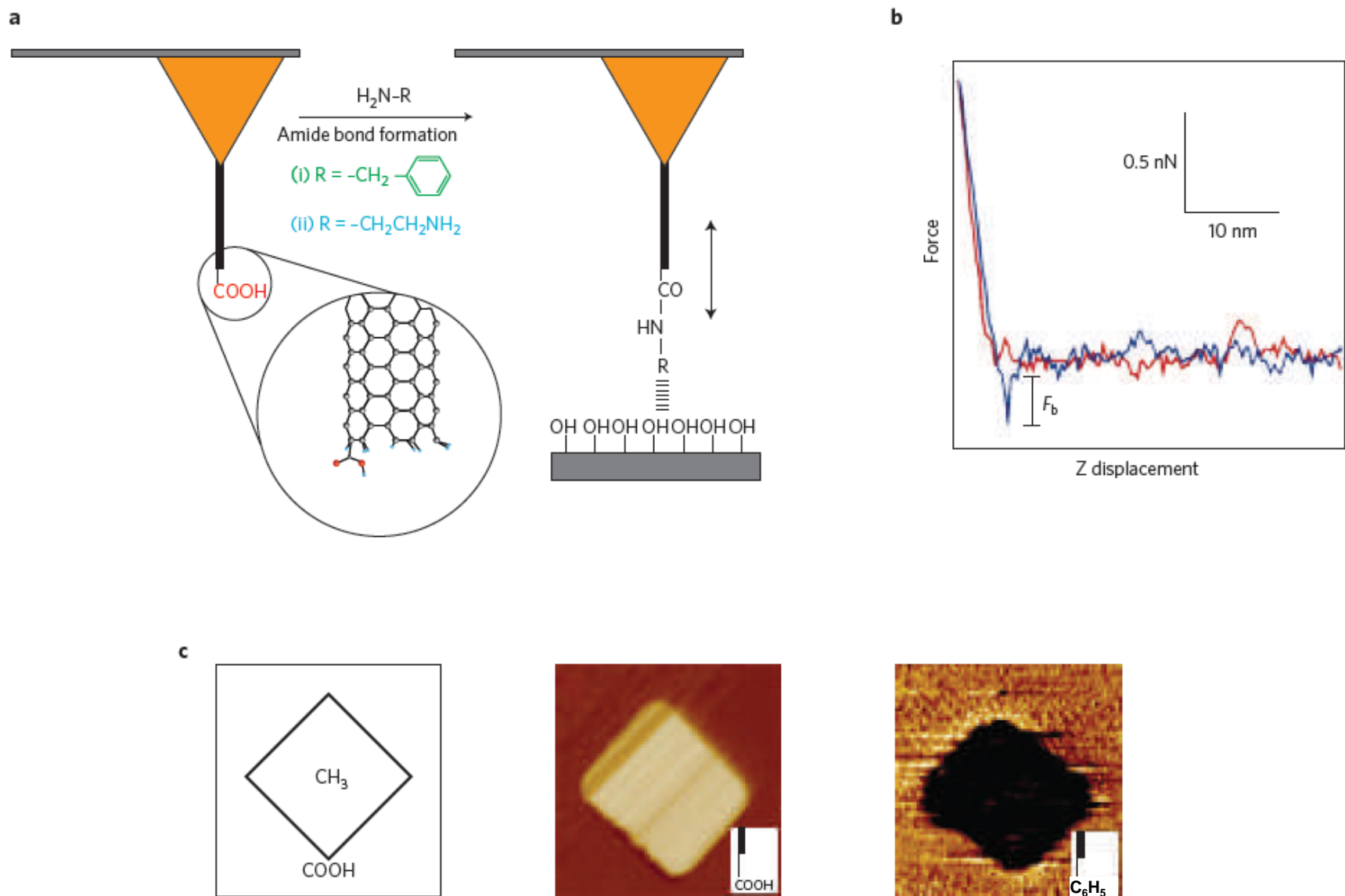


**Figure 5 | Production and application of chemically functionalized nanotube tips.** **a**, Schematic of the opened end of an oxidized SWNT tip and the carbodiimide coupling chemistry used in one form of chemical derivatization. **b**, A representative force-distance curve obtained with a biotin-modified SWNT tip on a streptavidin surface in solution; note that the binding force measured ( $\sim 200$  pN; blue line is the retract curve) corresponds to a single biotin-streptavidin chemical bond. **c**, Chemical imaging with functionalized nanotube tips. Left: Schematic of a patterned self-assembled monolayer terminating in methyl ( $\text{CH}_3$ ) and carboxyl ( $\text{COOH}$ ) end groups. Middle: Tapping-mode phase image of the patterned self-assembled monolayer shown in the left panel, obtained with a  $\text{COOH}$ -terminated tip. Right: Phase image of the same area obtained with a  $\text{C}_6\text{H}_5$ -terminated tip. Note the inversion in contrast. Figure reproduced with permission from ref. 49 (© 2000 Elsevier).

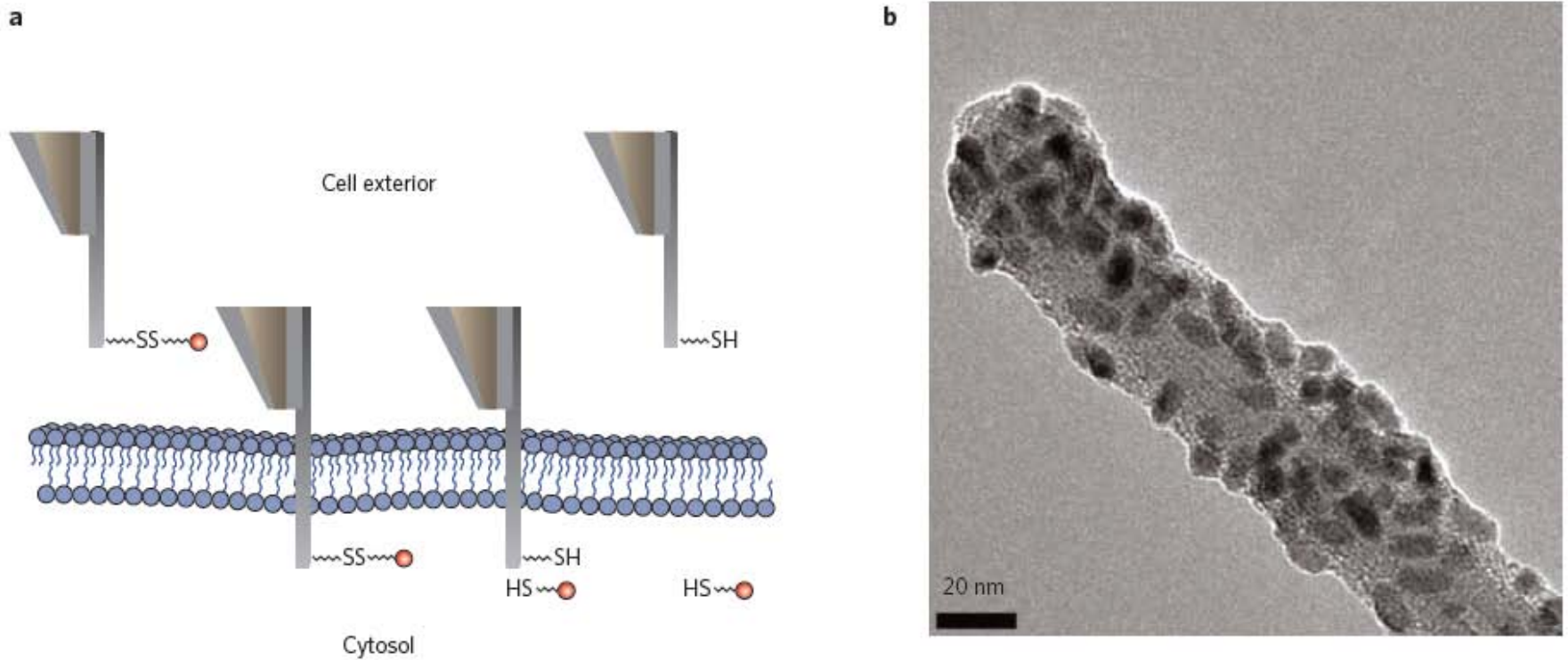


**Figure 6 | Schematic of the 'nanoinjection' procedure.** **a**, A MWNT-AFM tip with its cargo attached penetrates a cell membrane. On chemical stimulation the cargo is released and the nanoneedle is retracted. **b**, TEM image of a MWNT-AFM tip derivatized with quantum dots (the 'cargo'). Figure reproduced with permission from ref. 46 (© 2007 PNAS).

The needle-like nanotube tip was used to 'inject' **protein-coated quantum dots** into living human cells, crucially without significant physical disruption to the cell membrane or the nanotube.

The controlled release of a small number of target molecules into cells without physical damage could have far reaching implications for medical science and biotechnology

One example for nanotube-tip: as evidenced for improved imaging of DNA

---

**Single-Walled Carbon Nanotube AFM Probes: Optimal Imaging Resolution of Nanoclusters and Biomolecules in Ambient and Fluid Environments**

Liwei Chen,\* Chin Li Cheung, Paul D. Ashby, and Charles M. Lieber

*Department of Chemistry and Chemical Biology, Harvard University, Cambridge, Massachusetts 02138*

**NANO  
LETTERS**

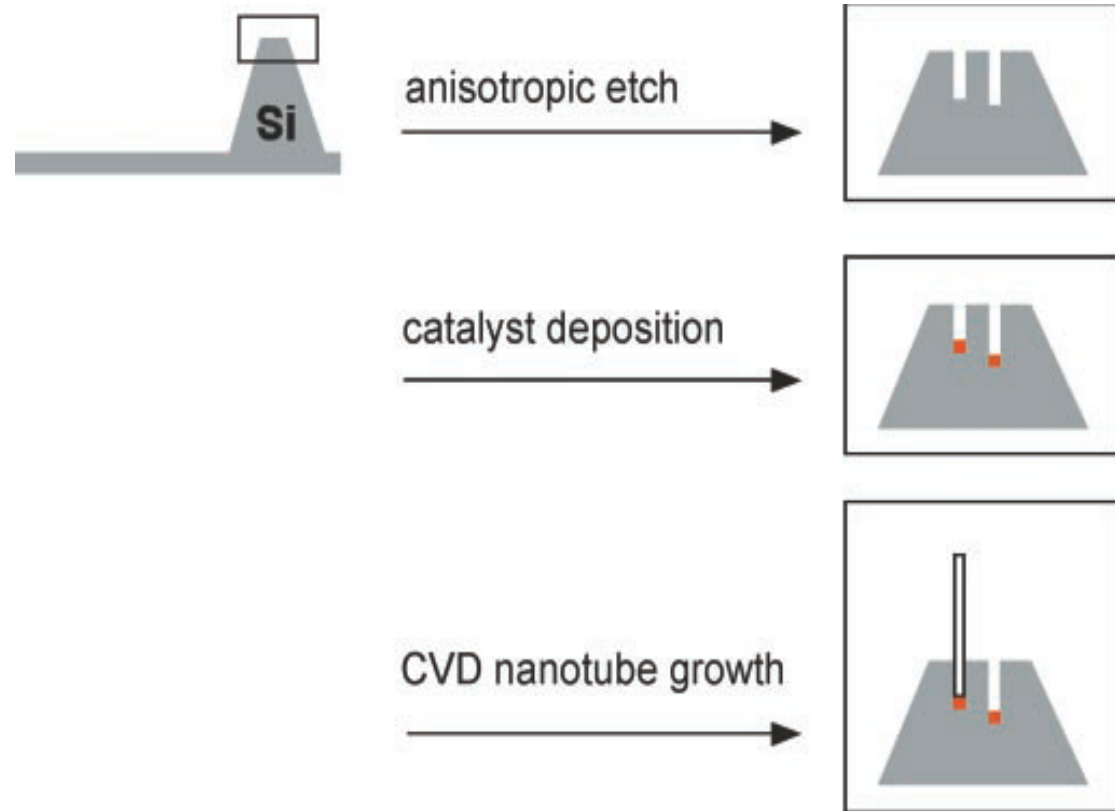
**2004  
Vol. 4, No. 9  
1725–1731**

# Individual SWNT Tip Preparation

**Method 1:** Direct surface growth of carbon nanotubes on AFM tips.  $\text{FeO}_x$  colloid catalyst was deposited onto commercial silicon FESP probes (force modulation etched silicon probe,  $k$ )

**Method 2:** The carbon nanotube “pick-up” method.  $\text{Fe}(\text{NO}_3)_3$  catalyst was deposited on oxidized silicon substrates and individual nanotubes were grown near normal to the surface

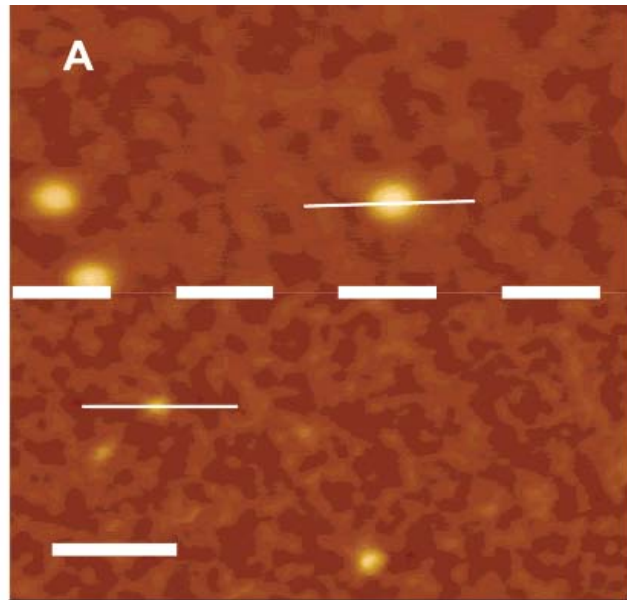
Nanotubes grown this way is more sustainable for repeated scanning, particularly in liquid.



Schematic of the CVD nanotube tip preparation approach.

# Carbon Nanotube Probe Imaging in Air

Gold nanocluster samples with diameters of  $5.2 \pm 1$  nm



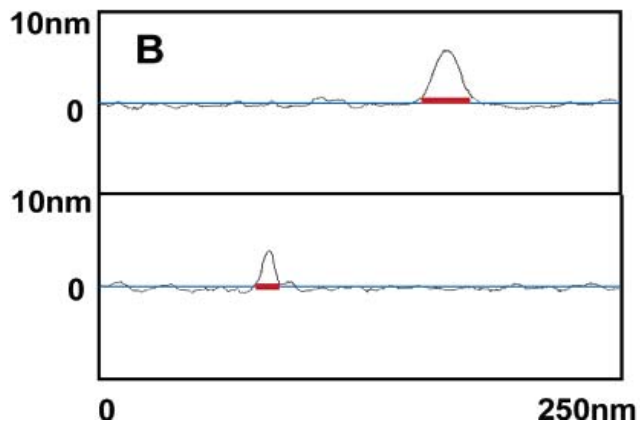
Gold nanoclusters imaged with SWNT tips in ambient conditions with a free oscillation amplitude ( $A_0$ ) of 40 nm.

The top section above the thick white dashed boundary line was imaged with an amplitude set point ( $A_{sp}$ ) of 37 nm.

The bottom section was imaged with an  $A_{sp}$  of 26 nm.

Scale bar is 50 nm.

Full width of the particle appears to be 26 nm at higher  $A_{sp}$  (37nm), and 10nm at lower  $A_{sp}$  (26nm). The diameter of SWNT probe is 3.5nm measured by TEM



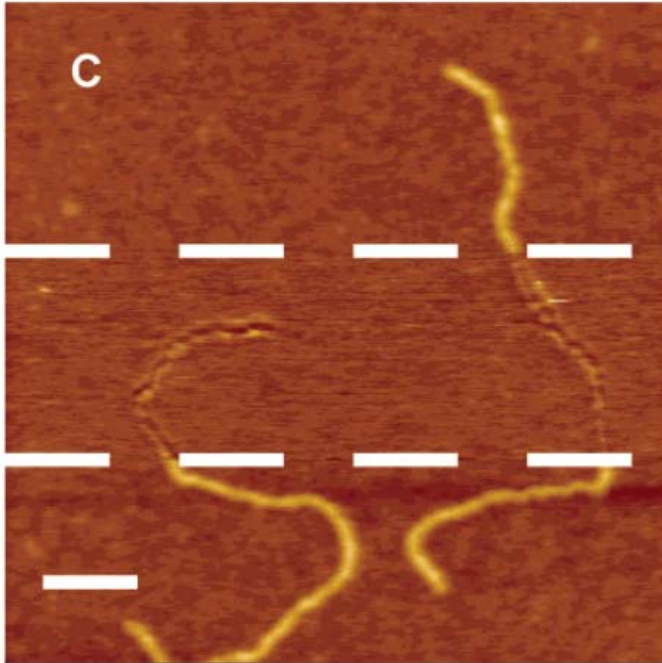
Measured size should be

$$\begin{aligned} &= 4 \times (R_{\text{sample}} \times R_{\text{tip}})^{0.5} \\ &= 4 \times (2.6 \times 1.75)^{0.5} = 8.5 \text{ nm} \end{aligned}$$

Quite close to the value as obtained above.

# Carbon Nanotube Probes Imaging in Air

1235 base pair linear DNA fragment



C. Isolated DNA molecules imaged with SWNT tips in ambient with an  $A_0$  of 42 nm.

The top and bottom section were imaged with an  $A_{sp}$  of 38 nm, whereas the midsection was imaged with an  $A_{sp}$  of 32 nm.

The scale bar is 50 nm.

D. Force calibration (FC) curves of the amplitude and phase channels for a SWNT tip imaging in ambient with an  $A_0$  of 42 nm.

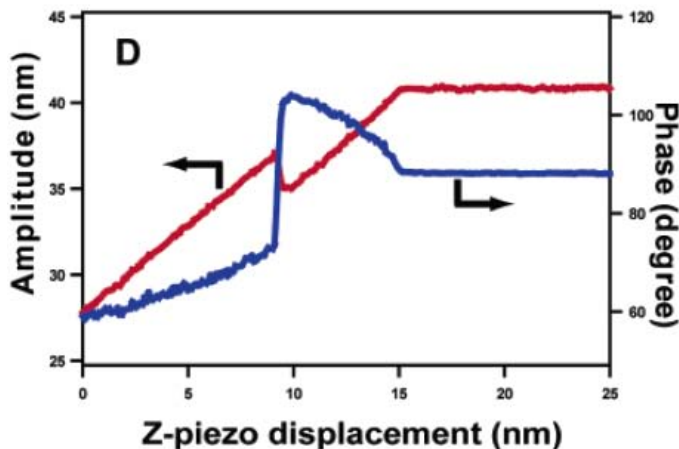
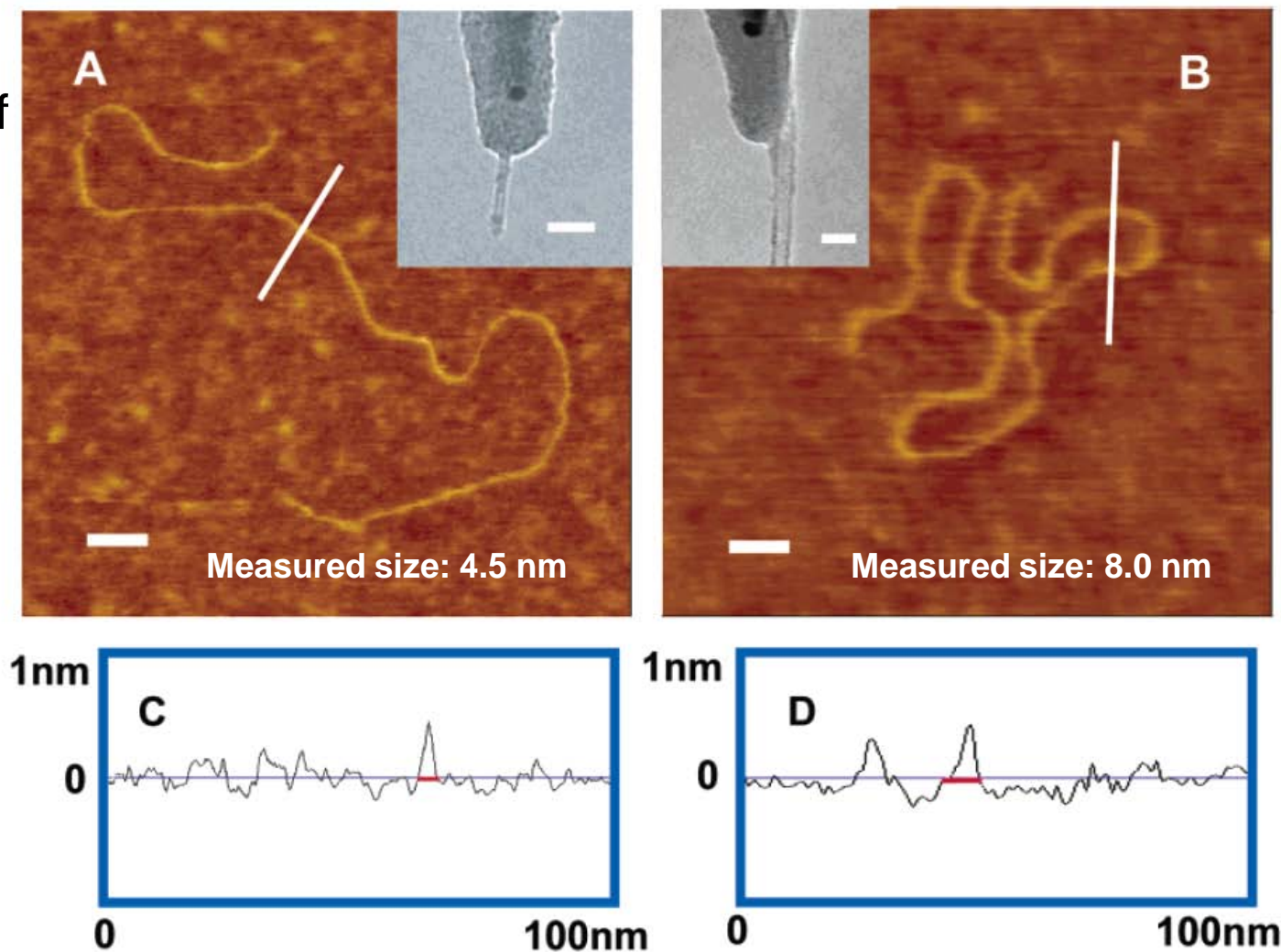



Exhibit a full width of **12nm** at a high  $A_{sp}$  of 38nm, and image is highly distorted with a low  $A_{sp}$  of 32nm. Low sample stiffness significantly limits AFM image resolution in ambient condition.

# Imaging of DNA in Fluid



**Figure 2.** (A and B) Isolated DNA molecules imaged with SWNT tips in water. Insets are TEM images of the corresponding SWNT tips used to obtain the AFM images in A and B, with tip diameters of 2.4 and 5.8 nm, respectively. The scale bars are 20 nm for the AFM images, and 10 nm for the insets. (C and D) The cross sections of the DNA imaged in A and B with full widths of  $4.5 \pm 0.2$  nm and  $8.0 \pm 0.3$  nm, respectively (the average width and standard deviations are obtained from 6 measurements).

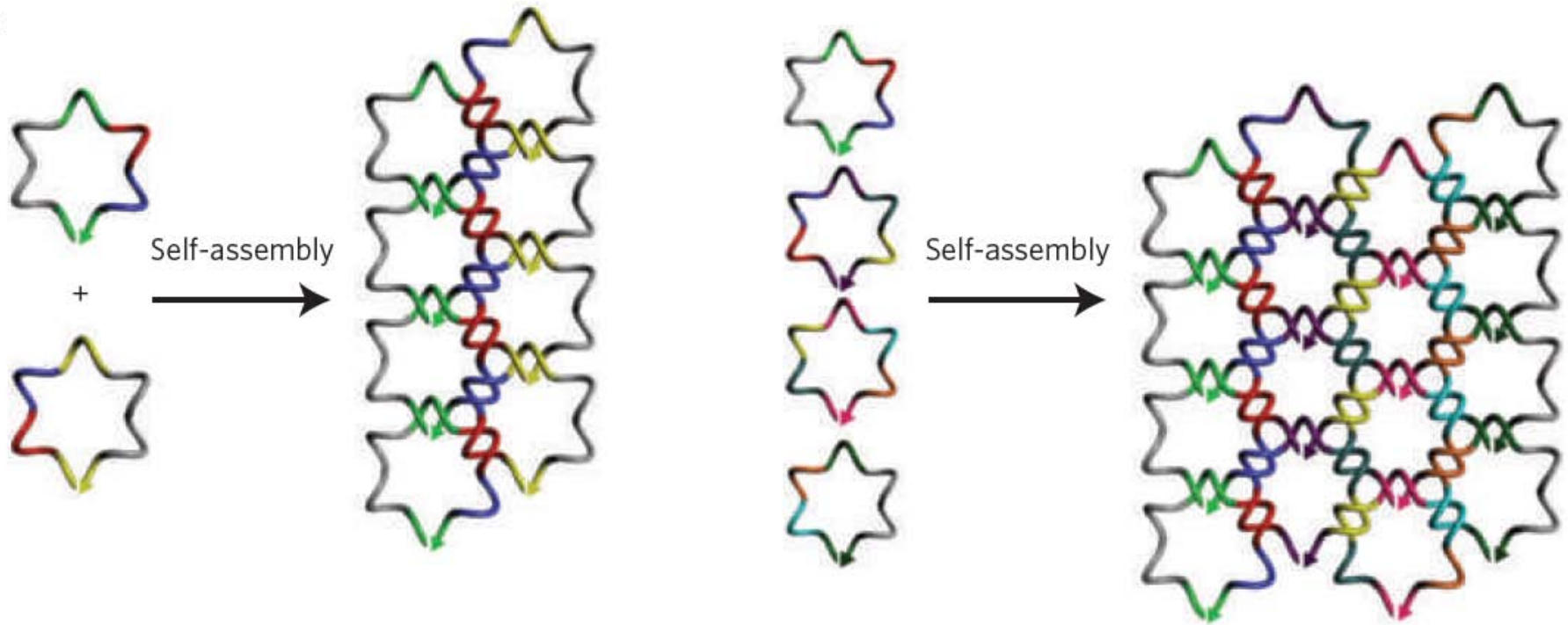
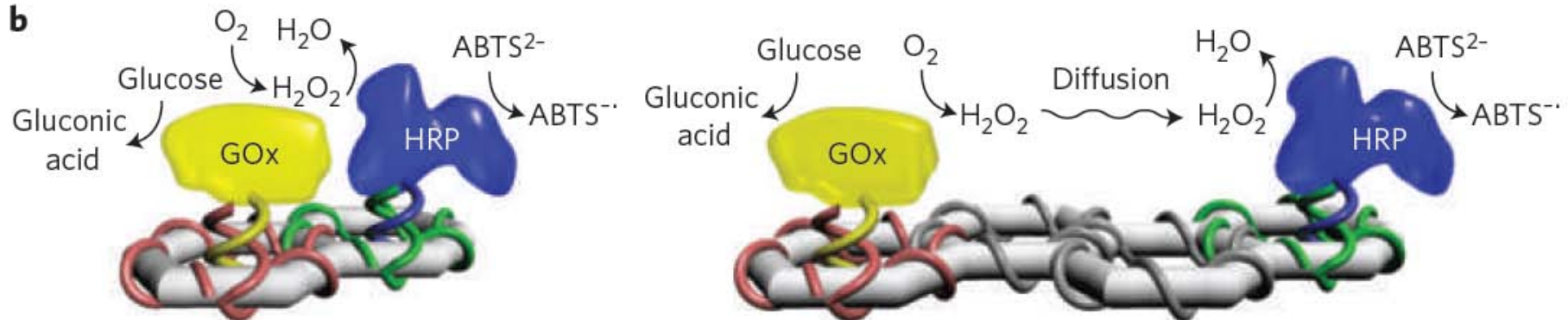
The geometry-limited tip-broadening of the DNA suggests that imaging in aqueous conditions belongs to the same regime as in ambient conditions with high  $A_0$  and low  $A_{sp}$ , even though the free oscillation amplitude in aqueous environment (2-5 nm) is extremely low compared to that in ambient (40 nm).

- 
- The following slides show the more sophisticated self-organized structures of DNAs, and the bio-related applications through templating or positioning.
  - See how high-resolution AFM imaging has been used in these studies, particularly to reveal the nanometer scale morphology

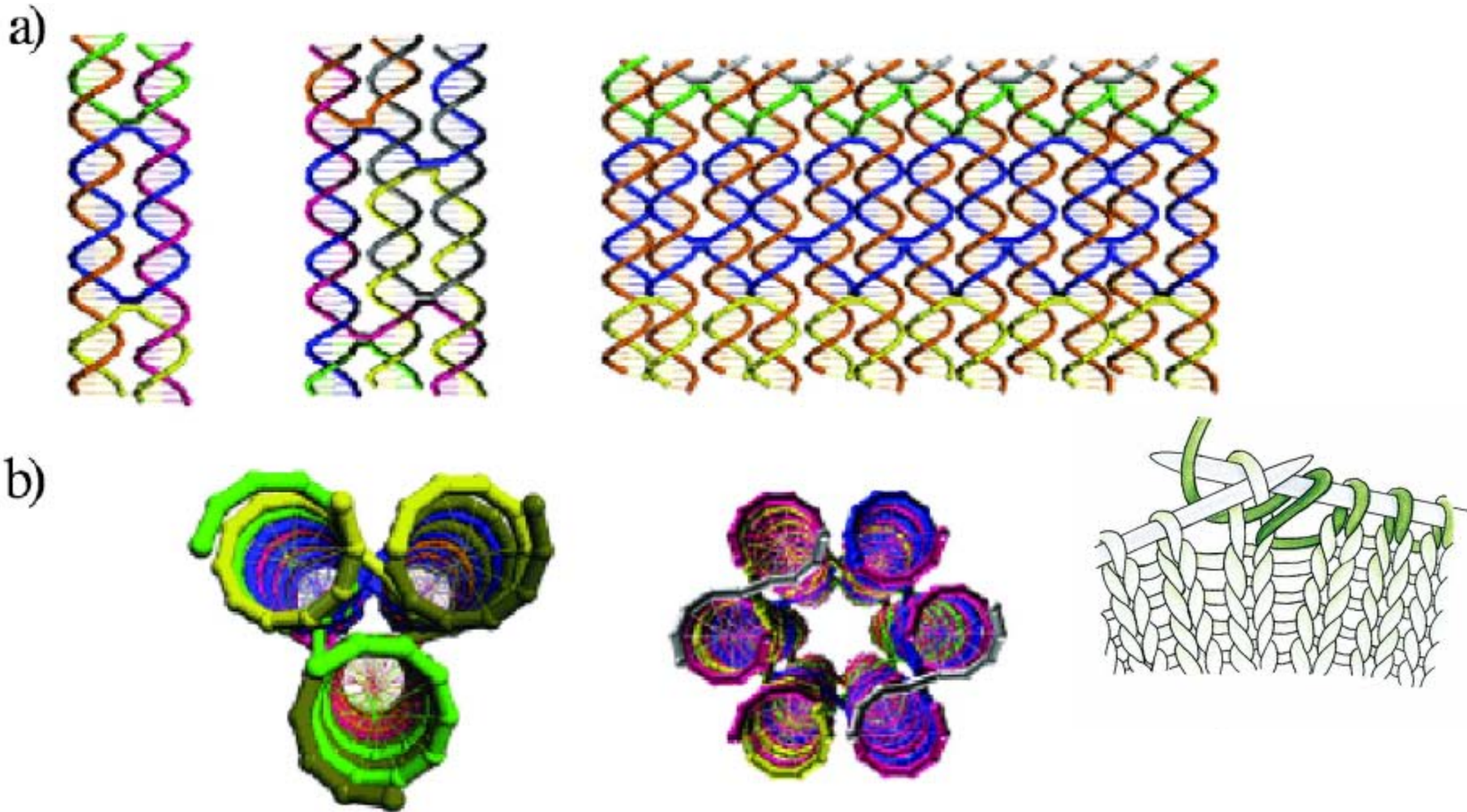


# A cascade of activity

Enzymatic reactions can be coupled together by carefully organizing the enzymes on DNA scaffolds.

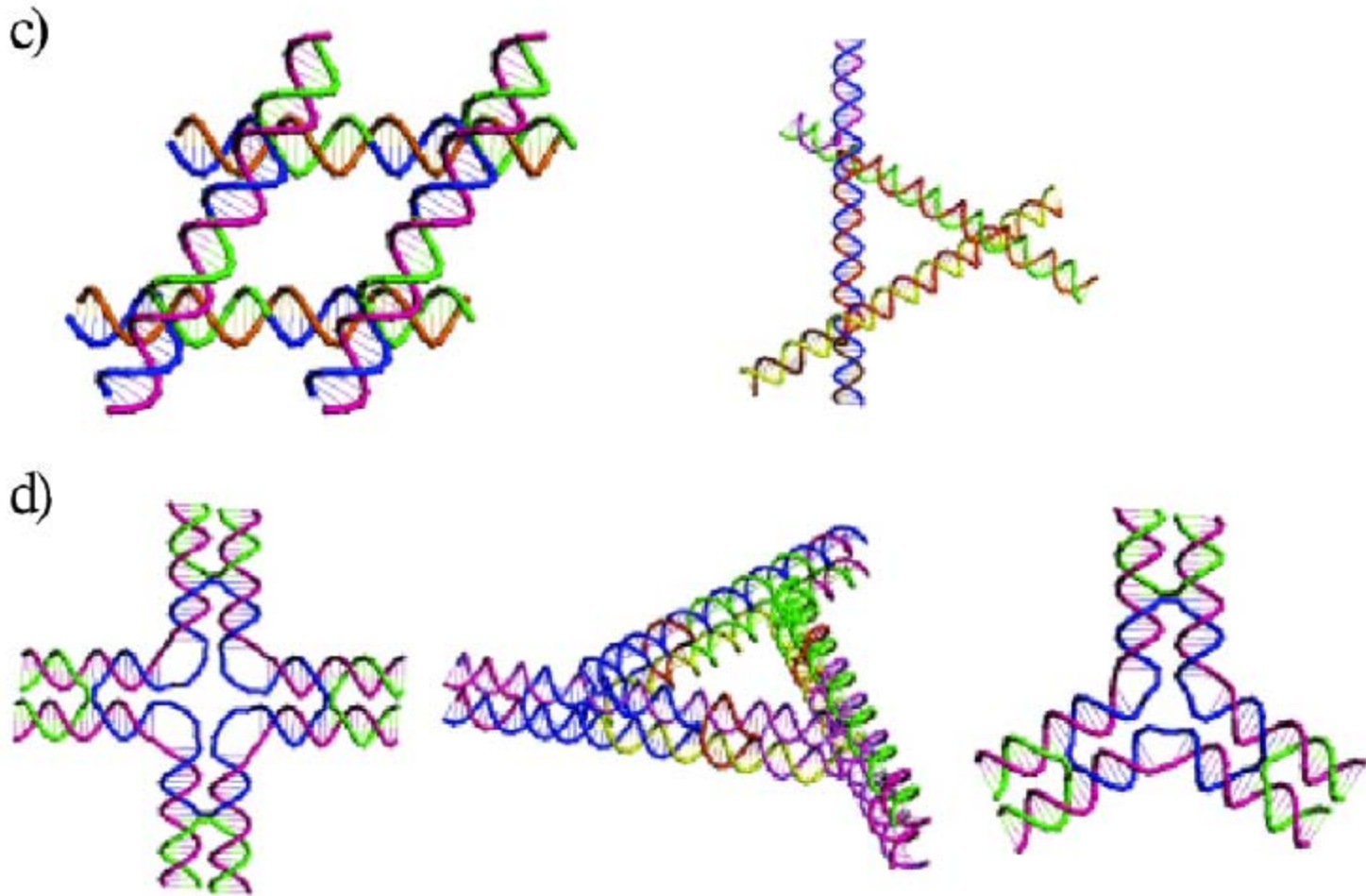
**a****b**

# The basic structural elements in DNA nanotechnology

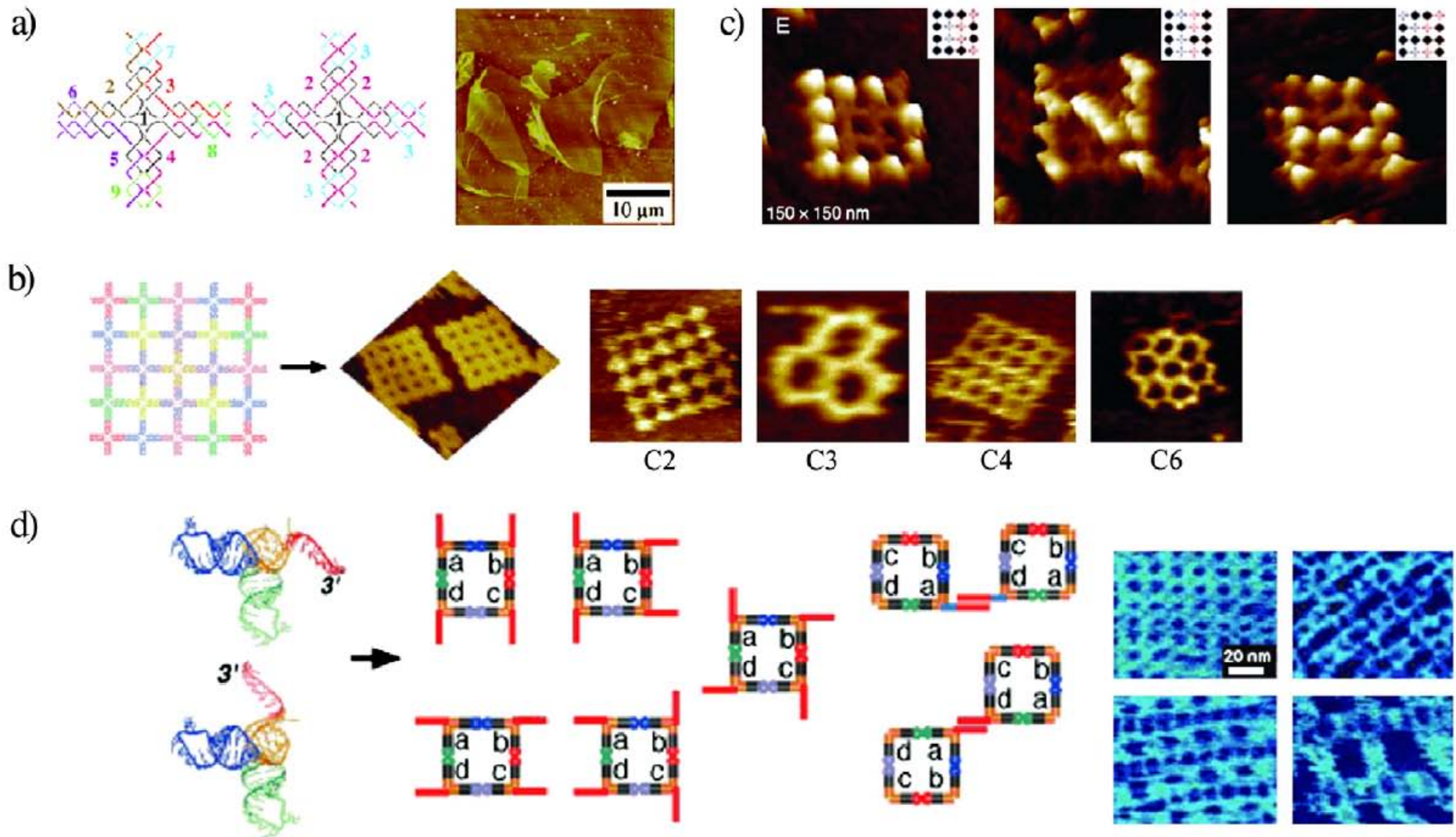


a) DX, TX, and 12 helix DNA tile; b) three and six helix bundles

# The basic structural elements in DNA nanotechnology

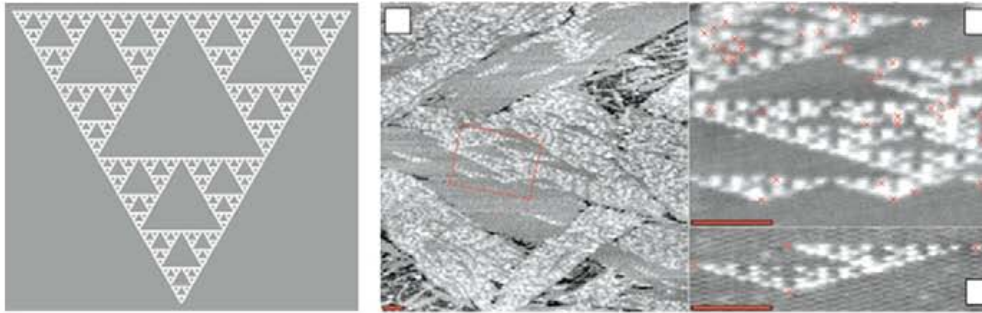


c) a parallelogram DNA tile with 4 four arm junctions and a triangle DNA tile with 3 four arm junctions; d) cross shaped tile, a DX based triangular DNA tile, 3 point star motif

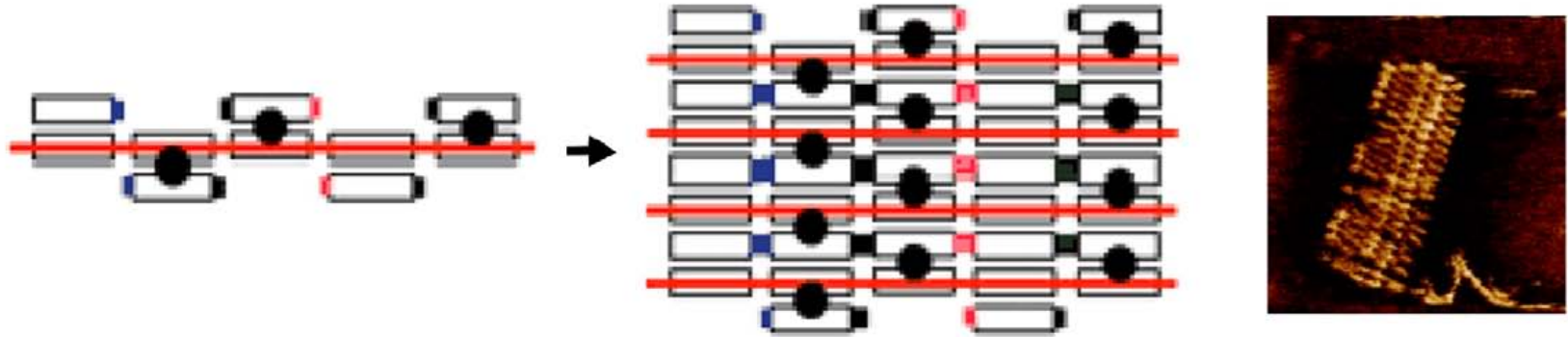


Examples of DNA nanostructures of different types and complexities; a) sequence symmetric arrays formed from cross-shaped tiles (adapted from ref. [37]); b) symmetric finite sized DNA arrays with C2, C3, C4 and C6 symmetries (adapted from ref. [19]); c) addressable finite-sized DNA scaffold, generated by hierarchical self-assembly process (adapted from ref. [20]); d) tecto-RNA assemble into tectosquares that form finite sized and two dimensional architectures with varying complexities (adapted from ref. [40])

e)



f)

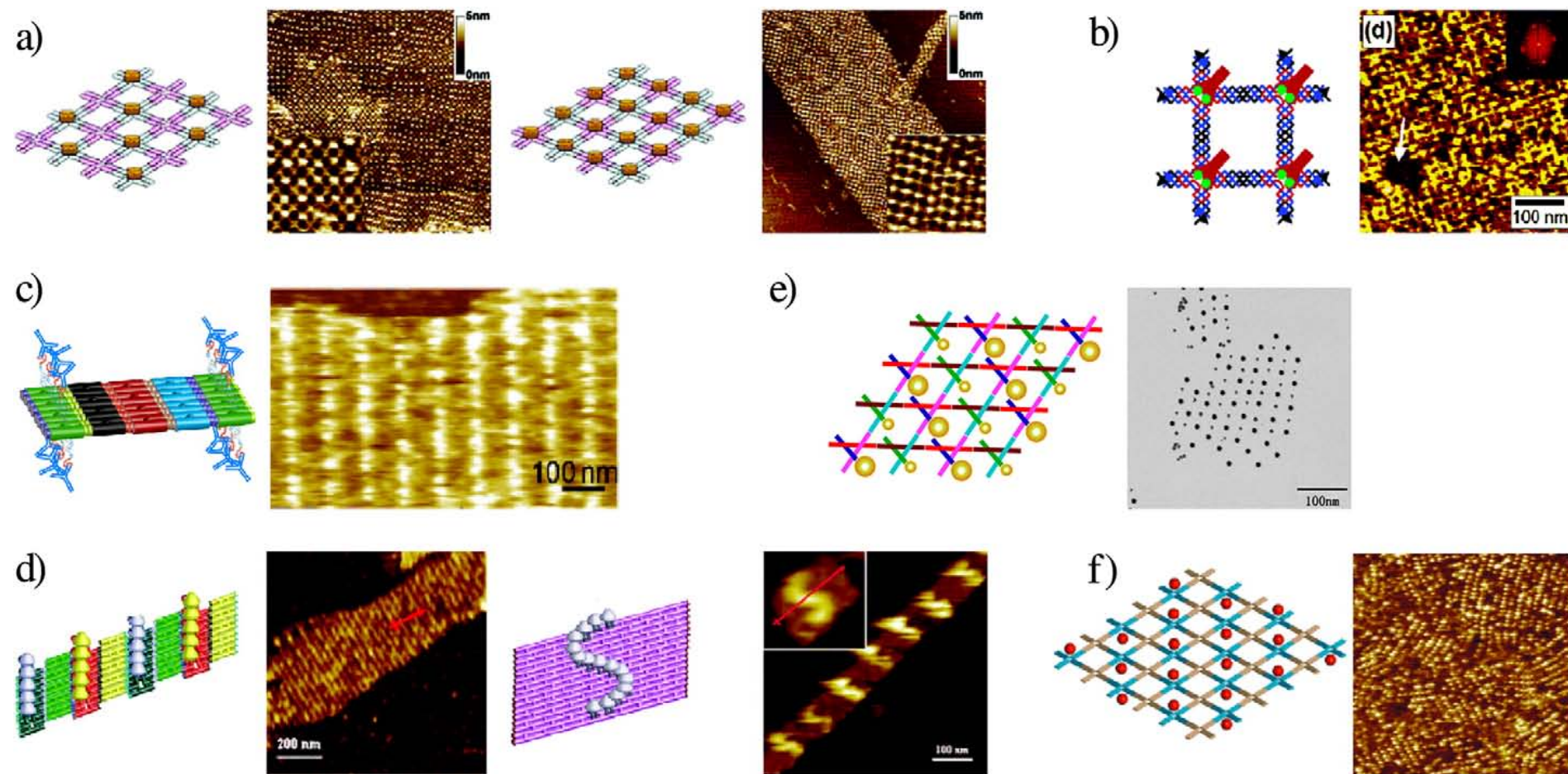


g)



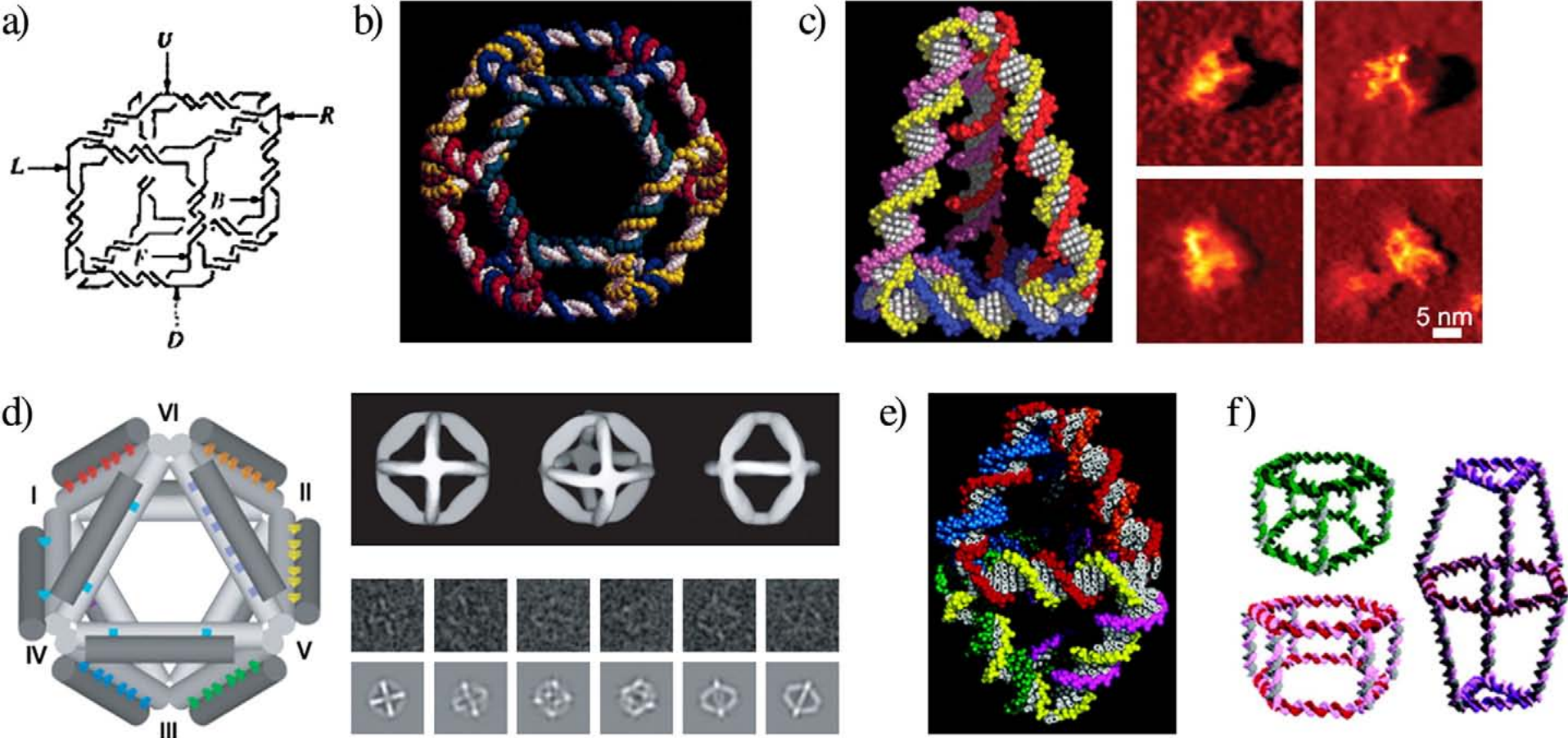
e) Sierpinski triangles, generated by algorithmic self-assembly process (adapted from ref. [21]); f) a DNA barcode lattice, assembled by nucleated self-assembly process (adapted from ref. [24] ; g) DNA origami, generated by nucleated self-assembly process, formed complex architectures (adapted from ref. [26]).

# DNA nanostructures as scaffolds for templating biomolecules and inorganic metallic nanoparticles,



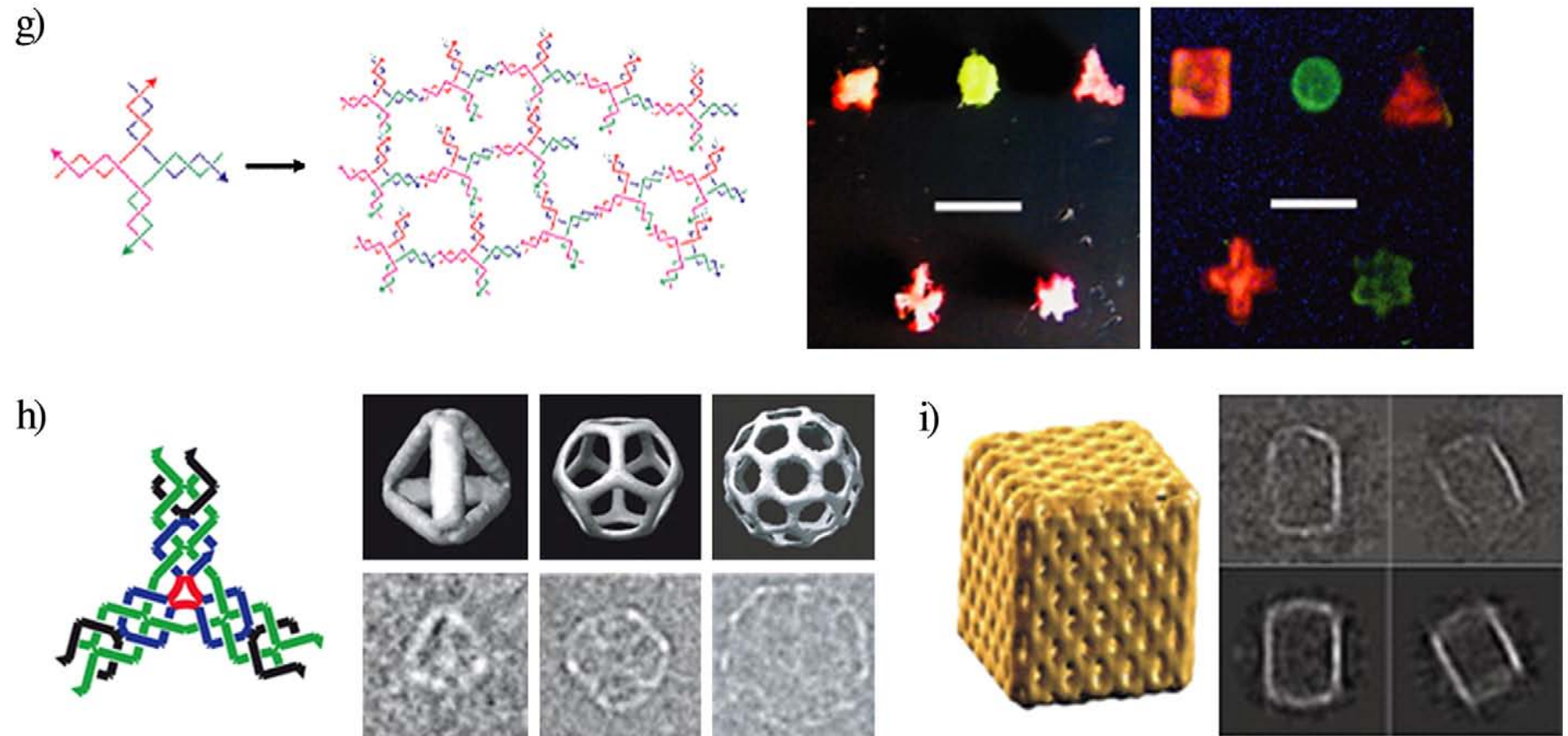
a) assembling streptavidin in a programmable manner by biotinylated DNA arrays (adapted from ref. [41]); b) Ordered arrays of antigens showing organization of antibodies in a periodic fashion (adapted from ref. [42]); c) Peptide arrays templated by DNA scaffold and antibody arrays (adapted from ref. [43]); d) aptamers directed complex and periodical multiprotein arrays, thrombin organized in 'S' manner by aptamer decorated complex DNA origami tile (adapted from ref. [49]); e) Multi-component system patterned by DNA scaffolds (adapted from ref. [52]); f) Two dimensional organization of gold nanoparticles templated by DNA scaffolds (adapted from ref. [53] J. Sharma, R. Chhabra, Y. Liu, Y. Ke and H. Yan, DNA-templated self-assembly of two-dimensional and periodical gold nanoparticles arrays, *Angew. Chem. Int. Ed.* **45** (5) (2006), pp. 730–735. [Full Text via CrossRef](#) | [View Record in Scopus](#) | [Cited By in Scopus \(97\)\[53\]](#)).

# Examples of 3D DNA objects and DNA supramolecular frameworks



a) schematic of the DNA cube generated through enzymatic ligations (adapted from ref. [33]); b) A DNA truncated octahedron (adapted from ref. [34]); c) DNA tetrahedron (adapted from ref. [35]); d) DNA octahedron generated by nucleated self-assembly process (adapted from ref. [25]); e) DNA bipyramid (adapted from ref. [36]); f) 3D DNA construction of pentaprisms, heptaprisms and biprisms (adapted from ref. [59] Y. He, T. Ye, M. Su, C. Zhang, A.E. Ribbe, W. Jiang and C. Mao, Hierarchical self-assembly of DNA into symmetric supramolecular polyhedra, *Nature* **452** (2008), pp. 198–202.[59]);

# Examples of 3D DNA objects and DNA supramolecular frameworks



g) a DNA based hydrogel self-assembled from X-DNA, based on DNA monomer type, different shape and size of gels can be assembled (adapted from ref. [63] S.H. Um, J.B. Lee, N. Park, S.Y. Kwon, C.C. Umbach and D. Luo, Enzyme-catalyzed assembly of DNA hydrogel, *Nat. Mater.* **5** (2006), pp. 797–801. [Full Text via CrossRef](#) | [View Record in Scopus](#) | [Cited By in Scopus \(43\)\[63\]](#)); h) Hierarchical self-assembly of tetrahedral, dodecahedra and buckyball from a three point star motif (adapted from ref. [60]); i) A 3D DNA box with controllable lid (adapted from ref. [61]).



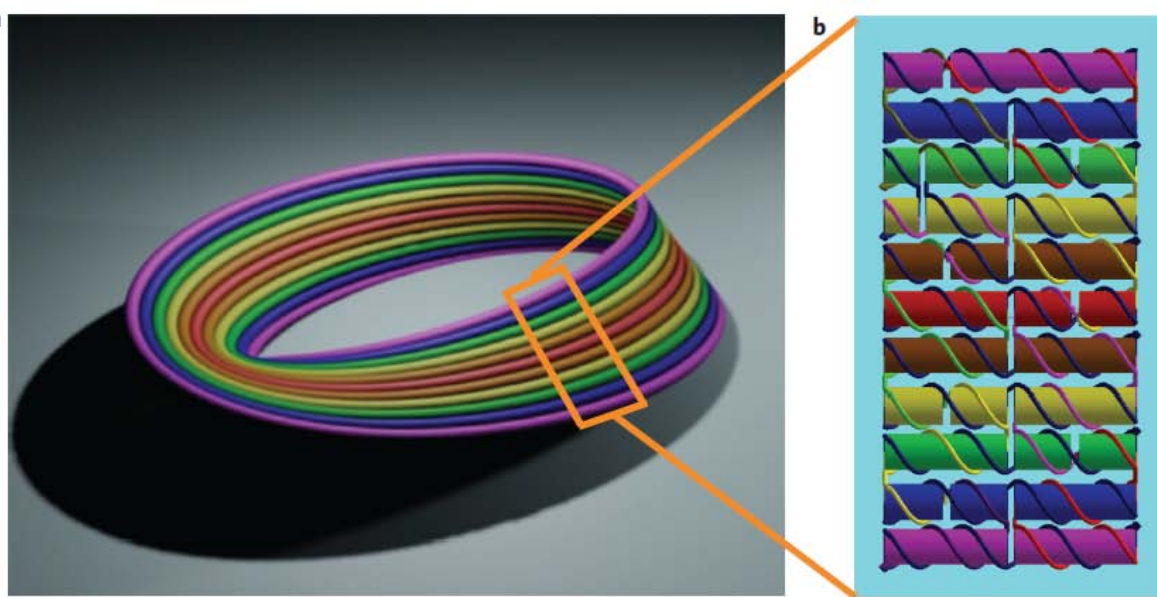
LETTERS

PUBLISHED ONLINE: 3 OCTOBER 2010 | DOI: 10.1038/NNANO.2010.193

nature  
nanotechnology

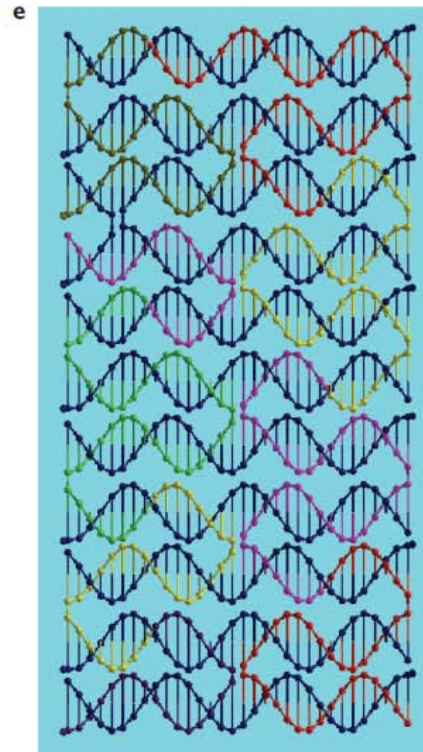
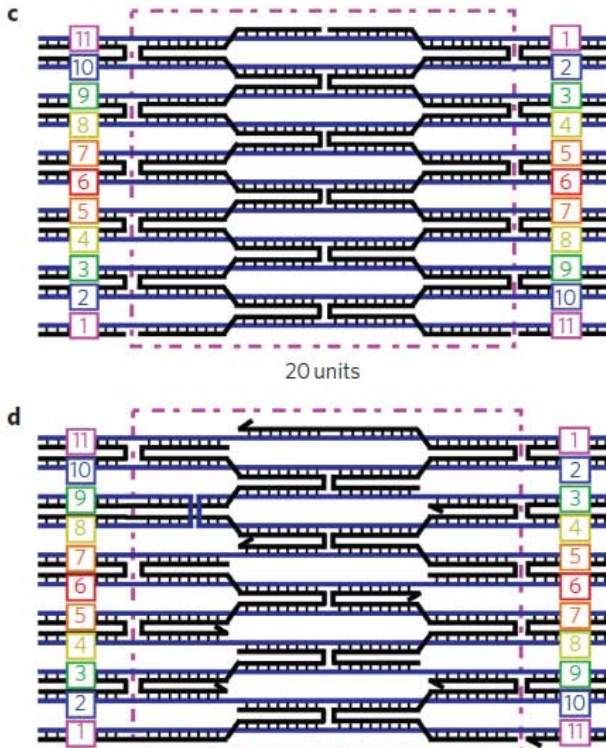
# Folding and cutting DNA into reconfigurable topological nanostructures

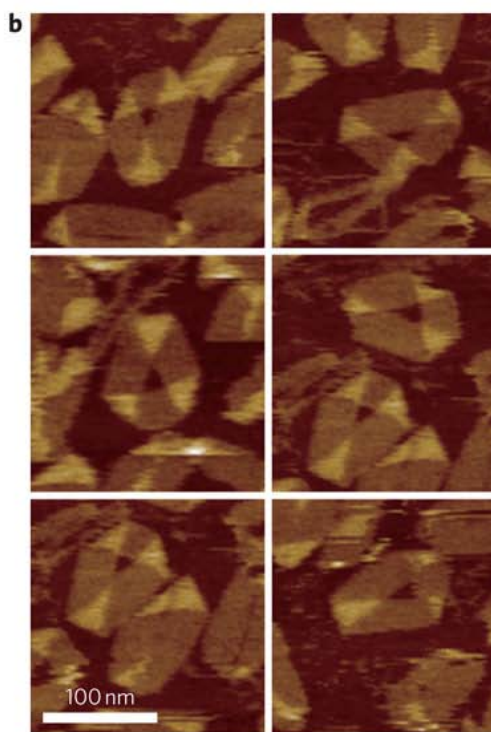
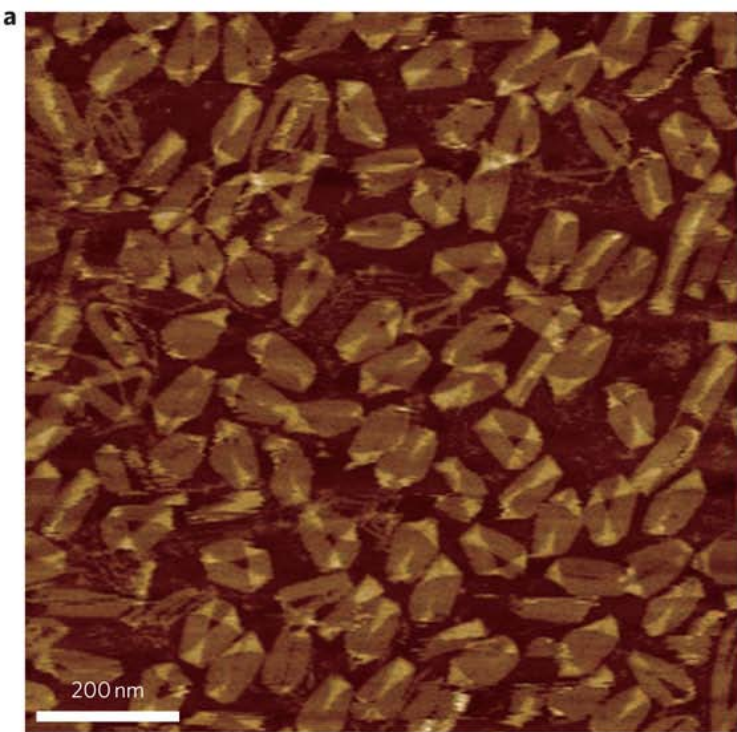
Dongran Han<sup>1,2</sup>, Suchetan Pal<sup>1,2</sup>, Yan Liu<sup>1,2\*</sup> and Hao Yan<sup>1,2\*</sup>



## Design of a Möbius DNA strip

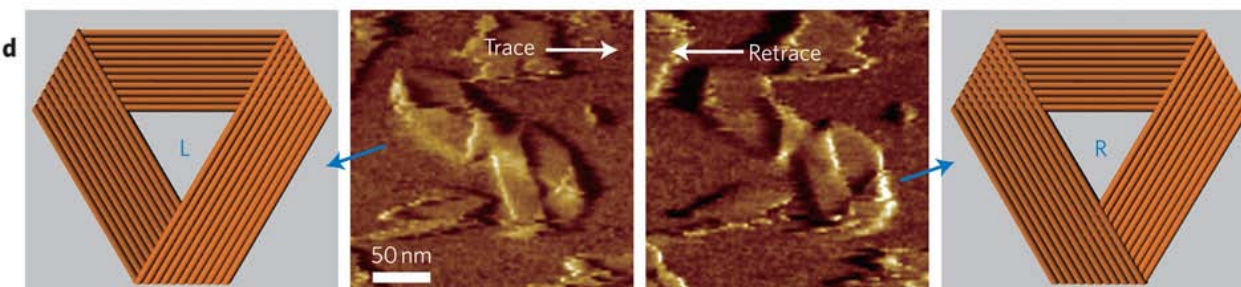
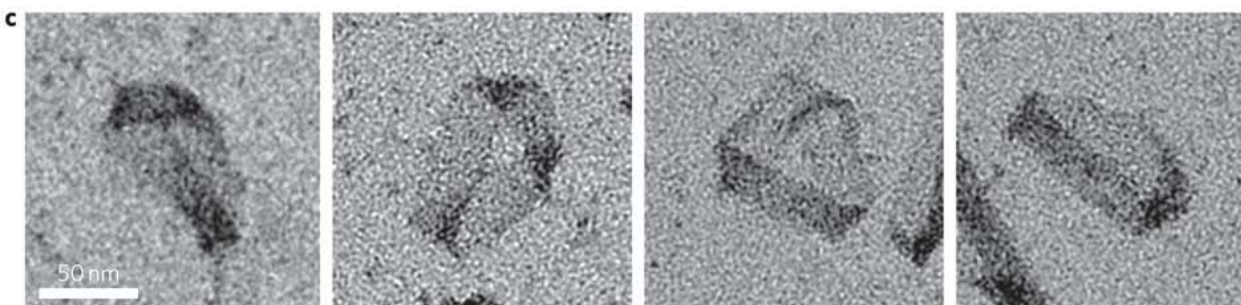
**a**, Three-dimensional illustration of the Möbius DNA strip. Each coloured band represents a different DNA double helix. **b**, A fraction of the Möbius strip in **a** is illustrated in the DNA helical model. The whole Möbius strip is composed of 20.5 of these units. **c**, Generalized folding path of a unit in the Möbius strip with the scaffold strand (blue) running through the entire structure and staple strands (black) helping to fold it into the designed structure. **d**, Design used in the experiment for one of the 20 units. The scaffold strand crosses over between helices 3 and 4. **e**, DNA helical strand model for the unit shown in **d**.





Visualization of the Möbius DNA strips with AFM and TEM imaging.

**a,b**, Zoom-out and zoom-in AFM images of the Möbius DNA strip. **c**, TEM images of the Möbius DNA strip negatively stained with uranyl formate. The two images on the left have a right-handed chirality, and the two images on the right have a left-handed chirality. **d**, AFM amplitude images with the tip scanning in trace and retrace directions indicating the co-existence of both left-handed and right-handed chiral structures in the sample. Schematics are shown to illustrate the chirality of the Möbius strip.



Nature Nanotechnology,  
p712–717, (2010)

DNA kirigami to achieve reconfigurable topologies from the Möbius strip.

**a–d**, DNA kirigami-ring structure: design schematics (**a,b**), AFM height images (**c**) and TEM images (**d**). **e–h**, The DNA kirigami-catenane structure: design schematics (**e,f**), AFM height (**g**, upper panels) and amplitude (**g**, lower panels) images, and TEM images (**h**)

